Pancreatic cancer cachexia is mediated by PTHrP-driven disruption of adipose *de novo* lipogenesis

Nikita Bhalerao[1,2], Yamini Ogoti[1,2], Jessica Peura[1,2], Calvin Johnson[1,2], Qingbo Chen[3], Ekaterina D. Korobkina[3], Faith N. Keller[4], Maximilian Wengyn[5], Robert J. Norgard[5], Claire Shamber[1,2], Kelsey Klute[6], Dominick DiMaio[7], Karine Sellin[8], Paul M. Grandgenett[9], Rui Li[10], Michael A. Hollingsworth[9], Adilson Guilherme[11], Michael P. Czech[11], Richard Kremer[8], Lihua Julie Zhu[2,3,10], Emma V. Watson[4], Marcus Ruscetti[2], David A. Guertin[3], Jason R. Pitarresi[1,2]

[1] Division of Hematology-Oncology, Department of Medicine, University of Massachusetts Chan Medical School, Worcester, MA, USA

[2] Department of Molecular, Cell and Cancer Biology, University of Massachusetts Chan Medical School, Worcester, MA, USA

[3] Program in Molecular Medicine, University of Massachusetts Chan Medical School, Worcester, MA, USA

[4] Department of Systems Biology, University of Massachusetts Chan Medical School, Worcester, MA, USA

[5] Abramson Family Cancer Research Institute and Department of Medicine, University of Pennsylvania, Philadelphia, PA, USA

[6] Department of Internal Medicine, University of Nebraska Medical Center, Omaha, NE, USA

[7] Department of Pathology and Microbiology, College of Medicine, University of Nebraska Medical Center, Omaha, NE, USA

[8] Division of Endocrinology and Metabolism, Department of Medicine, McGill University and McGill University Health Centre, Montréal, Quebec, Canada.

[9] Eppley Institute for Research in Cancer and Allied Diseases, Fred and Pamela Bufferr Cancer Center, University of Nebraska Medical Center, Omaha, NE, USA

[10] Department of Genomics and Computational Biology, University of Massachusetts Chan Medical School, Worcester, MA, USA

[11] Program in Molecular Medicine, Diabetes Center of Excellence, University of Massachusetts Chan Medical School, Worcester, MA, USA

Corresponding author: J.R. Pitarresi; Jason.Pitarresi@umassmed.edu

Conflict of interest statement: The authors declare no potential conflicts of interest. RK is the inventor of the therapeutic monoclonal anti-PTHrP antibodies used in this study and authorized for use by Miramab Bioscience. RK holds an equity stake in Miramab Bioscience.

Running Title: PTHrP drives pancreatic cancer cachexia

Keywords: Pancreatic cancer, PTHrP, PTHLH, cancer cachexia, adipose wasting**,** *de novo* lipogenesis, DNL

ABSTRACT

Pancreatic cancer patients have the highest rates and most severe forms of cancer cachexia, yet cachexia etiologies remain largely elusive, leading to a lack of effective intervening therapies. PTHrP has been clinically implicated as a putative regulator of cachexia, with serum PTHrP levels correlating with increased weight loss in PDAC patients. Here we show that cachectic PDAC patients have high expression of tumor PTHrP and use a genetically engineered mouse model to functionally demonstrate that deletion of *Pthlh* (encoding the PTHrP protein) blocks cachectic wasting, dramatically extending overall survival. The re-expression of PTHrP in lowly cachectic models is sufficient to induce wasting and reduce survival in mice, which is reversed by the conditional deletion of the PTHrP receptor, *Pth1r*, in adipocytes. Mechanistically, tumor-derived PTHrP suppresses *de novo* lipogenesis in adipocytes, leading to a molecular rewiring of adipose depots to promote wasting in the cachectic state. Finally, the pharmacological disruption of the PTHrP-PTH1R signaling axis abrogates wasting, highlighting that a targeted disruption of tumor-adipose crosstalk is an effective means to limit cachexia.

STATEMENT OF SIGNIFICANCE

Pancreatic ductal adenocarcinoma (PDAC) is the prototypical cancer type associated with cancer cachexia, a debilitating wasting syndrome marked by adipose tissue loss and muscle atrophy. Herein, we establish that PTHrP is a tumor-derived factor that facilitates cachexia by downregulating *de novo* lipogenesis in adipocytes and that blocking PTHrP is an effective means to limit wasting in preclinical mouse models.

INTRODUCTION

Pancreatic cancer ranks as the third most fatal cancer in the United States, surpassed only by lung cancer and colorectal cancer [1]. The lack of robust treatment options and early detection opportunities for Pancreatic Ductal Adenocarcinoma (PDAC) patients contribute to a dismal 5-year survival rate of ~13% [2]. In addition, PDAC patients often present with cancer-associated cachexia, a systemic metabolic syndrome marked by profound adipose tissue and muscle wasting, which impacts body condition and tolerance to available treatment options, thus contributing to reduced survival rates. A striking >75% of PDAC patients suffer from cachexia [3], with nearly one-third of PDAC-associated deaths being attributable to cachexia rather than tumor burden [4]. The perturbed metabolic state in cachectic patients across cancer types has been proposed to be mediated by various tumor-derived factors, such as IL-6 [5], Parathyroid Hormone-Related Protein (PTHrP) [6], TNFα [7], and GDF15 [8, 9], that likely act in concert to alter tumor-host interactions and facilitate wasting.

Clinically, cachexia presents as a multifactorial metabolic syndrome characterized by loss of body weight due to wasting of adipose tissue and muscle mass [10]. Despite patients often presenting with anorexia and anemia, nutritional supplementation does little to curtail weight loss and extend survival [11]. Thus, it is clear from clinical evidence and preclinical models that cachexia is a comorbidity in cancer and that a deeper understanding of the molecular basis of cancer-associated cachexia is required to find new ways to treat cachectic patients and, ultimately, extend survival. Additionally, how tumors communicate with peripheral tissues such as adipose and muscle is largely

unexplored and represents an untapped area to apply targeted therapy to block cachectic wasting.

Adipose tissue loss has been shown to precede muscle loss in cachectic PDAC patients [12], nominating tumor-adipose crosstalk as a potential point of therapeutic intervention. Under normal physiological conditions, white adipocytes have unilocular lipid droplets and are involved in energy storage and mobilization. During cachexia, some white adipocytes shift their metabolism towards an energy-expending state that resembles thermogenesis [12]. This shift from a primarily energy-storing organ to an energy-consuming organ is a hallmark of adipose tissue wasting in cancer cachexia, yet few tumor-derived factors have been nominated as putative regulators of this crosstalk. Canonically, this metabolic shift has been attributed to an upregulation of adipocyte lipolysis, or the breaking down of fatty acids [13-15]. However, emerging work suggests that decreased *de novo* lipogenesis (DNL) may also contribute to adipose tissue loss in this context [16].

To better understand the molecular etiology of cancer cachexia and associated adipose tissue wasting, we employ a murine model of pancreatic cancer that is accompanied by severe cachexia. We identify PTHrP as a PDAC tumor-derived factor that promotes cancer-associated adipose wasting marked by profound downregulation of *de novo* lipogenesis, and provide pre-clinical evidence to support anti-PTHrP therapy as a cachexia blocking strategy.

RESULTS

70 ***Tumor cell-specific Pthlh deletion extends overall survival and reduces PDAC-associated cachexia***

72 The conditional expression of *Kras*$^{LSL\text{-}G12D}$ and *Trp53*$^{LSL\text{-}R172H}$ were targeted to the murine pancreas using the *Pdx1-Cre* allele, as previously described [17]. The addition of a

74 Rosa26$^{LSL\text{-}YFP}$ lineage label allows for the tracking of tumor cells derived from the Pdx1 lineage [18]. The resulting ***K****ras*$^{LSL\text{-}G12D}$; *Tr****p****53*$^{LSL\text{-}R172H}$; *Pdx1-****C****re*; Rosa26$^{LSL\text{-}\underline{Y}FP}$ (KPCY)

76 mice were combined with the *Pthlh*^{LoxP} allele (*Pthlh* gene encodes the PTHrP protein) to delete *Pthlh* specifically in tumor cells (Supplemental Figure 1A). Our prior work revealed

78 a genetic linkage between *Kras* and *Pthlh* (these genes are directly adjacent in the mouse and human genome), which precludes the inheritance of homozygous *Pthlh*$^{LoxP/LoxP}$

80 alleles in combination with *Kras*$^{LSL\text{-}G12D}$ [19]. Nonetheless, the heterozygous deletion of *Pthlh* in KPCY mice (KPCY-Pthlh^{HET}) dramatically extended survival compared to KPCY

82 controls, with KPCY-Pthlh^{HET} mice living ~2.5 months longer (Figure 1A). KPCY-Pthlh^{HET} mice survived a median of 187 days, a ~68% extension of survival relative to the KPCY

84 median survival of 111 days, which we had previously attributed to reduced metastatic ability [19]. Upon closer examination of the overall body condition of KPCY-Pthlh^{HET}

86 animals, we also observed that they were less cachectic than their KPCY counterparts. To quantify cachexia, body weights were tracked in an age-matched cohort of KPCY and

88 KPCY-Pthlh^{HET} mice in the 15 days prior to sacrifice. KPCY mice underwent significant cachectic wasting over time, while KPCY-Pthlh^{HET} mice, on average, continued to gain or

90 maintain their body mass (Figure 1B). At endpoint, the mouse carcass weights were increased in KPCY-Pthlh^{HET} mice relative to KPCY controls (Figure 1C).

To profile more deeply the degree of cachectic wasting in these animals, inguinal white adipose tissue (iWAT), epididymal white adipose tissue (eWAT), and quadricep (quad) muscle were collected across two cohorts; the first set of tissue was collected when mice reached endpoint (Figure 1D-F), and the second cohort at a set endpoint of 5 months (Figure 1G-I). At endpoint, KPCY-Pthlh^{HET} mice showed reduced iWAT, eWAT, and quad wasting (Figure 1D-F). Similarly, in the age-matched 5-month-old cohort, KPCY-Pthlh^{HET} mice showed reduced iWAT, eWAT, and quad wasting (Figure 1G-I). Strikingly, KPCY-Pthlh^{HET} adipose and muscle tissue masses were more similar to those of non-tumor bearing (NTB) animals, suggesting that the loss of tumor cell-derived PTHrP blocked cachectic wasting. Histopathologically, the adipose tissue of KPCY mice was highly cachectic, with marked remodeling of the adipose architecture and a reduction in adipocyte lipid droplet size (Figure 1D-E and 1G-H). In contrast, iWAT and eWAT from KPCY-Pthlh^{HET} mice more closely resembled that of NTB hosts and were primarily composed of large unilocular adipocytes (Figure 1D-E and 1G-H). Quad muscle morphology was also perturbed in KPCY mice, while muscle from KPCY-Pthlh^{HET} mice was more similar to NTB (Figure 1F and 1I). Cachectic muscle from KPCY mice had increased expression of the E3 ubiquitin ligases *Trim63* (MURF1) and *Fbxo32* (ATROGIN1) that mediate muscle wasting [20], which were lost in KPCY-Pthlh^{HET} mice (Supplemental Figure 1B). To precisely quantify the cachectic burden in adipose tissue, we measured adipocyte size, a proxy for the lipid storing capacity of adipocytes. Adipocyte size was reduced in the iWAT from *KPCY* mice (indicative of adipose wasting), while KPCY-Pthlh^{HET} adipocytes were larger and more similar in size to NTB animals

(Figure 1J; Supplemental Figure 1C). Fluorescent staining of iWAT with the adipocyte lipid
116 droplet marker PLIN1 indicated that overall lipid size was reduced in cachectic KPCY mice, which returned to normal in non-cachectic KPCY-Pthlh^{HET} mice (Figure 1K).

118

Importantly, overall tumor burden did not correlate with the degree of adipose
120 (Supplemental Figure 1D; Pearson R^2=0.002) or muscle wasting (Supplemental Figure 1E; Pearson R^2=0.015) across our cohort of KPCY orthotopic and GEMM animals,
122 consistent with prior reports demonstrating that tumor burden does not dictate the degree of cancer-associated cachexia in other models [21, 22]. In fact, we often observed
124 relatively small tumors (~500-750mg) that were highly cachectic and much larger tumors (>2 grams) that showed no evidence of cachectic wasting (Supplemental Figure 1D-E).
126 Taken together, the varying degree of PDAC-associated cachexia in genetically identical *KPCY* tumor bearing animals indicates that the ability to induce cachexia is a tumor cell-
128 intrinsic trait, and we have identified highly cachectic and lowly cachectic KPCY tumor cell clones to test putative cachexia-inducing tumor-derived factors such as PTHrP.

130

Prior work has established that cachectic PDAC patients have higher serum PTHrP
132 relative to non-cachectic patients [23]. We hypothesized, based on our prior work, that PTHrP is coming from PDAC tumor cells [19], and set out to determine if high PTHrP
134 tumor expression corresponds with cachectic burden in a cohort of cachectic and non-cachectic PDAC patients. Indeed, levels of PTHrP in primary tumors from cachectic
136 PDAC patients were increased relative to non-cachectic PDAC patients (Figure 1L), and we have previously demonstrated that increased PTHrP staining in primary tumors

138 correlates with decreased survival of PDAC patients [19]. Collectively, these data show that PTHrP mediates adipose and muscle wasting cachectic phenotypes in genetically
140 engineered mouse models of pancreatic cancer and that PTHrP is increased in cachectic PDAC patients, setting the stage for mechanistic studies to determine the role of tumor-
142 derived PTHrP in the induction of pancreatic cancer cachexia.

144

Pthlh overexpression is sufficient to induce cachexia

146 The genetic deletion of PTHrP reduced cachexia phenotypes, demonstrating that it is necessary for PDAC-associated cachectic wasting. To determine if PTHrP is sufficient to
148 induce wasting, we took a lowly cachectic KPCY cell line with low basal expression of *Pthlh* (Supplemental Figure 2A) and stably re-expressed *Pthlh* (PTHrP^{OE}) via lentiviral-
150 mediated transduction (Supplemental Figure 2B). The resulting KPCY-PTHrP^{OE} tumor cells had a modest, but statistically significant increase in tumor cell proliferation *in vitro*
152 relative to empty vector expressing cells (KPCY-EV; Supplemental Figure 2C), consistent with our prior reports [19]. Upon orthotopic implantation, the re-expression of *Pthlh*
154 significantly reduced overall survival (Figure 2A) and was sufficient to induce a dramatic cachectic phenotype, effectively converting a non-cachectic PDAC cell line into a
156 cachectic one (Figure 2B). Consistent with the induction of cachexia, iWAT architecture was altered upon *Pthlh* overexpression (Figure 2C), and iWAT mass was greatly reduced
158 in KPCY-PTHrP^{OE} tumor bearing animals relative to isogenic KPCY-EV controls (Figure 2D). Adipocyte size was also reduced (Figure 2E; Supplemental Figure 2D) with a
160 concomitant reduction in PLIN1-positive lipid droplet size in iWAT from KPCY-PTHrP^{OE}

mice (Figure 2F). Similarly, muscle architecture was perturbed, and muscle mass was
162 reduced in KPCY-PTHrP^{OE} tumor bearing mice (Figure 2G-H). Murf1 (*Trim63*) and Atrogin1 (*Fbxo32*) expression were increased in cachectic muscle from KPCY-PTHrP^{OE}
164 tumor bearing hosts relative to those with KPCY-EV tumors (Supplemental Figure 2E).

166 KPCY-PTHrP^{OE} tumors were larger than KPCY-EV tumors (Supplemental Figure 2F), potentially complicating the interpretation that PTHrP is driving wasting phenotypes. To
168 control for this, we repeated the experiment in an independent cohort where primary tumors were size matched (Supplemental Figure 2G), by harvesting mice at day 18 for
170 KPCY-EV tumors and day 10 for KPCY-PTHrP^{OE} tumors. Despite having less time to induce cachexia, KPCY-PTHrP^{OE} tumor bearing animals showed increased adipose
172 wasting phenotypes in iWAT (Supplemental Figure 2H). At this early time point, quad weights were not significantly different (Supplemental Figure 2I), highlighting that adipose
174 wasting precedes muscle wasting in this model and that PTHrP directly mediates adipose wasting. Finally, to demonstrate that PTHrP acts directly on adipose tissue, we injected
176 NTB C57BL/6 animals with recombinant PTHrP (rPTHrP), which was sufficient to decrease iWAT mass after just 5 days of treatment (Figure 2I-J). These results indicate
178 that tumor cell-derived PTHrP is sufficient to induce PDAC-associated cachexia, primarily by facilitating adipose wasting.

180

182 ***Adipocyte-specific deletion of Pth1r attenuates PDAC-associated cachexia***

To decouple tumor growth and energy consumption cachectic phenotypes from direct
184 tumor-adipocyte crosstalk mediated wasting, we set out to disrupt PTHrP signaling by conditionally deleting its cognate receptor, Parathyroid Hormone 1 Receptor (*Pth1r*), in
186 cachectic tissue. Analysis of the Genotype-Tissue Expression (GTEX) database indicated that amongst tissues that undergo wasting in cachexia (adipose, skeletal muscle, heart,
188 etc.), adipose tissue has the highest levels of *PTH1R* expression, with very little to no expression in skeletal muscle (Figure 3A; all tissues shown in Supplemental Figure 3A).
190 To confirm this phenomenon in mice, we isolated RNA from multiple organs of non-tumor bearing C57BL/6 mice and performed qPCR for *Pth1r*, which indicated that adipose tissue
192 depots were the most highly expressing organ that undergoes cachectic wasting (Figure 3B). Of note, *Pth1r* levels are highest in the kidney, consistent with previous studies [24]
194 and likely unrelated to cachectic wasting. Additionally, analysis of a single-cell atlas of human adipose tissue [25] indicated that *PTH1R* is most highly expressed in adipocytes
196 and pre-adipocytes (adipose stem and progenitor cells or ASPCs; Figure 3C), suggesting that adipocyte lineages are the most likely cell in adipose tissue to respond to tumor-
198 derived PTHrP. Similar results were seen in the murine adipose tissue single-cell atlas [25], with *Pth1r* being most highly expressed in adipocytes and pre-adipocytes
200 (Supplemental Figure 3B). Immunofluorescent staining of adipose tissue indicated that PTH1R is expressed in adipocytes and is increased in cachectic animals (Figure 3D).
202 Collectively, this indicated that PTH1R is highly expressed in adipocytes and is likely to mediate PTHrP-PTH1R tumor to adipose crosstalk.
204

To functionally interrogate the role of the PTHrP-PTH1R signaling axis in cachectic
206 wasting, we deleted *Pth1r* specifically in adipocytes (i.e. *Adiponectin-Cre; Pth1r*$^{LoxP/LoxP}$ mice, herein *Pth1r*$^{Adipo\text{-}cKO}$). When implanted with KPCY-PTHrP^{OE} tumors, adipose tissue
208 wasting was reduced in *Pth1r*$^{Adipo\text{-}cKO}$ mice relative to WT hosts, with the loss of *Pth1r* in adipocytes blocking tumor-induced morphological changes to the adipose tissue (Figure
210 3E-F). *Pth1r*$^{Adipo\text{-}cKO}$ tumor bearing hosts exhibited increased lipid droplet size (Figure 3G-H; Supplemental Figure 3C), indicating that cachectic adipose tissue wasting was
212 reduced when PTHrP-PTH1R signaling in adipocytes is disrupted. Remarkably, blocking PTHrP-PTH1R tumor to adipocyte signaling preserved muscle architecture and reduced
214 wasting (Figure 3I-J). In KPCY-PTHrP^{OE} tumor bearing mice, Murf1 (*Trim63*) and Atrogin1 (*Fbxo32*) expression were increased in cachectic muscle from WT hosts, which was
216 reduced in *Pth1r*$^{Adipo\text{-}cKO}$ hosts (Supplemental Figure 3D). Thus, tumor cell-secreted PTHrP initiates PTH1R-mediated adipose and muscle wasting.

218

PTHrP-mediated adipose tissue wasting downregulates de novo lipogenesis

220 To determine the downstream mechanism by which PTHrP-PTH1R signaling axis mediates cachectic adipose wasting, we performed bulk RNA-sequencing (RNA-seq)
222 analysis on iWAT from cachectic (KPCY-PTHrP^{OE}) and non-cachectic (KPCY-EV) tumor bearing mice (Figure 4A). Cachectic adipose tissue from KPCY-PTHrP^{OE} tumor bearing
224 animals and non-cachectic adipose tissue from KPCY-EV clustered separately by differential gene expression analysis (Supplemental Figure 4A) and Principal Component
226 Analysis (PCA; Supplemental Figure 4B), indicating broad transcriptomic changes between the groups, consistent with the striking morphological changes we observed in

228 the cachectic tissues. The top 50 differentially expressed downregulated genes in KPCY-PTHrP^{OE} tumor bearing hosts relative to KPCY-EV tumor bearing hosts were comprised
230 of known regulators of adipocyte cell biology, including *Fasn*, *Pnpla3*, *Nnat*, and *Orm1* (Supplemental Figure 4C; Supplemental Table 1). The top upregulated genes consisted
232 of immune cell markers such as *Marco*, *Ccr6*, and *Cxcr5* (Supplemental Figure 4C; Supplemental Table 1).

234

Gene set enrichment analysis (GSEA) indicated that adipose from highly cachectic KPCY-
236 PTHrP^{OE} tumor bearing animals upregulated hallmark mediators of cancer cachexia, such as the TNF-α and IL-6 pathways (Figure 4B-C) [10], consistent with the cachexia-
238 inducing ability of PTHrP [26] . Surprisingly, in addition to these known pro-cachectic pathways, the adipose from KPCY-PTHrP^{OE} tumor bearing animals dramatically
240 downregulated adipogenesis and fatty acid metabolism pathways (Figure 4B-C), suggesting a perturbed regulation of lipid homeostasis in adipocytes during cachexia.
242 Consistent with this pathway analysis, key fatty acid metabolism genes were markedly downregulated in the adipose of highly cachectic animals, including a downregulation of
244 *de novo* lipogenesis (DNL) enzymes (*Acss2*, *Acly*, *Acaca*, and *Fasn*), lipases (*Lep*, *Lipe*, *Pbpla2*, *Plin1/2*), and fatty acid metabolism genes (*FABPs*, *Prdm16*, *Ppargc1a*, *Elovl6*)
246 (Figure 4D). The vast majority of DNL pathway components were downregulated in the adipose from cachectic KPCY-PTHrP^{OE} mice relative to non-cachectic KPCY-EV control
248 mice (Figure 4E; red arrows indicate downregulated genes). Notably, *Fasn* was the most significantly downregulated DNL gene (Figure 4A) and one of the top 15 overall

250 downregulated genes (Supplemental Figure 4C). Thus, tumor-derived PTHrP significantly downregulates adipose DNL to putatively facilitate cachectic wasting.

252

Adipocyte specific disruption of de novo lipogenesis sensitizes adipose tissue to
254 ***wasting***

To confirm that DNL pathway components were downregulated in response to PTHrP, we
256 performed qPCR on adipose tissue from PTHrP-overexpressing tumor bearing animals, which showed lower *Acss2*, *Acly*, *Acaca*, and *Fasn* expression (Figure 5A). Western
258 blotting analysis further confirmed the downregulation of DNL enzymes in cachectic iWAT (Figure 5B). Finally, qPCR demonstrated that master transcriptional regulators of DNL,
260 *Mlxipl* (ChREBPα and CHREBPβ isoforms) and *Srebf1c* (SREBP), were downregulated in the adipose of PTHrP-overexpressing tumor bearing mice (Figure 5C).

262

To determine the functional role of DNL in PDAC-associated adipose tissue wasting, we
264 implanted the non-cachectic KPCY PDAC line in *Adiponectin-Cre; Fasn*$^{LoxP/LoxP}$ mice (herein *Fasn*$^{Adipo\text{-}cKO}$; knockout confirmed in iWAT in Supplemental Figure 5A). In this
266 context, the loss of adipocyte *Fasn* resulted in perturbed tissue histology and significantly reduced adipose tissue mass (Figure 5D-E), demonstrating that the disruption of DNL in
268 adipose tissue is sufficient to prime the cachectic state. In addition to worsened adipose tissue wasting, *Fasn*$^{Adipo\text{-}cKO}$ tumor bearing animals had reduced adipocyte size (Figure
270 5F; Supplemental Figure 5B) and smaller PLIN1-positive lipid droplets (Figure 5G). Loss of adipose *Fasn* did not alter primary tumor growth (Supplemental Figure 5C) or quad
272 wasting or pathology (Supplemental Figure 5D-E). Collectively, this data shows a

previously unappreciated role for DNL in regulating PDAC-associated adipose tissue
274 wasting.

276 ***Anti-PTHrP therapy blocks PDAC-associated cachexia***

No effective therapies currently exist to treat PDAC-associated cachexia. Given our
278 genetic data indicating that the deletion of tumor cell *Pthlh* or adipocyte *Pth1r* reduces cachexia, we set out to determine if anti-PTHrP therapy is an effective means to disrupt
280 PTHrP-PTH1R tumor-adipose crosstalk and block cachectic wasting in PDAC. We have previously demonstrated that monoclonal neutralizing antibodies directed against PTHrP
282 (anti-PTHrP) effectively block PTHrP signaling in PDAC tumor cells, reducing primary tumor burden and metastatic ability [19]. To test the efficacy of anti-PTHrP as a cachexia-
284 blocking therapy in autochthonous KPCY tumors, we enrolled mice when their tumors reached 75 mm^3, at which point we began anti-PTHrP or anti-IgG antibody treatment.
286 Anti-PTHrP therapy normalized adipose tissue architecture (Figure 6A), reduced adipose wasting (Figure 6B), and increased adipocyte lipid size (Figure 6C; Supplemental Figure
288 6A) in KPCY mice. Anti-PTHrP treatment of KPCY mice trended towards increased quad mass and normalized morphology (Figure 6D-E). Murf1 (*Trim63*) and Atrogin1 (*Fbxo32*)
290 were mildly induced in the muscles of tumor-bearing animals at this stage, with anti-PTHrP antibody reducing their expression (Supplemental Figure 6B). Similar to the
292 GEMMs, the treatment of orthotopic KPCY tumors (from a cachectic clonal KPCY cell line) with anti-PTHrP therapy showed a similar reduction in cachexia phenotypes, with
294 normalization of the adipose tissue architecture (Figure 6F), reduced adipose tissue wasting (Figure 6G), and increased lipid droplet size (Figure 6H; Supplemental Figure

296 6C). Additionally, anti-PTHrP treated orthotopic tumor-bearing animals had reduced muscle wasting phenotypes (Figure 6I-J). The muscles of anti-IgG-treated orthotopic mice
298 showed evidence of modest Murf1 (*Trim63*) and Atrogin1 (*Fbxo32*) induction, which was reduced in anti-PTHrP-treated mice (Supplemental Figure 6D). Both KPCY GEMMs and
300 orthotopic tumor bearing animals treated with anti-PTHrP had increased lipid droplet size as visualized by PLIN1 staining of iWAT (Figure 6K-L). Finally, RNA-seq was performed
302 on iWAT from anti-PTHrP (or anti-IgG control) treated orthotopic KPCY tumor bearing animals. Similar to the genetic disruption of PTHrP-PTH1R signaling, anti-PTHrP
304 treatment reduced pro-inflammatory TNF-α signaling and enhanced adipogenesis and fatty acid metabolism signaling pathways in adipose tissue (Figure 6M). Similarly, iWAT
306 from anti-PTHrP treated animals upregulated *Fasn* (Figure 6N) and other DNL enzymes (Supplemental Figure 6E) relative to anti-IgG. Thus, anti-PTHrP monoclonal antibody
308 therapy is an effective means to reduce cachexia in multiple PDAC mouse models, primarily through a reduction in adipose tissue wasting phenotypes by restoring DNL
310 pathway expression.

312 **DISCUSSION**

Pancreatic cancer remains the lowest 5-year survival rate amongst the common cancers,
314 in large part due to the highest prevalence and severity of cancer cachexia [3]. Cachectic wasting of both the adipose and muscle reduces PDAC patients' quality of life and overall
316 survival [4, 27], and there are very few treatment options for the clinical management of cancer cachexia. To effectively manage cachexia in the clinic, new therapeutic targets
318 must be identified that directly mediate wasting phenotypes. In our prior work, we identified the oncogenic and pro-metastatic molecule PTHrP as a tumor-derived secreted
320 factor that correlates with decreased survival in human PDAC patients and whose genetic deletion or pharmacological inhibition in PDAC mouse models greatly enhances survival
322 [19]. Herein, we expand upon these initial findings to show that PTHrP is responsible for PDAC-associated adipose tissue wasting in cachexia (Figure 7). Thus, targeting PTHrP
324 therapeutically may be a multi-pronged attack to simultaneously block cancer cachexia, tumor growth, and metastasis. We show that cachectic patients have higher tumor PTHrP
326 expression relative to non-cachectic patients, and that the genetic deletion or pharmacological inhibition of PTHrP reduces cachectic wasting and enhances overall
328 survival in mouse models of PDAC-associated cancer cachexia. Induced expression of *Pthlh* in a lowly cachectic PDAC tumor cell line was sufficient to induce adipose and
330 muscle wasting, ultimately leading to reduced overall survival in mice. Disruption of PTHrP-PTH1R tumor to adipose crosstalk via adipocyte-specific conditional deletion of
332 *Pth1r* reduced adipose and muscle wasting, demonstrating that direct tumor cell to adipocyte signaling networks mediate adipose wasting that ultimately fuels muscle
334 wasting. Mechanistically, we found that cachectic adipose tissues lose core DNL signaling

components while concomitantly upregulating pro-cachectic factors such as TNF-α and IL-6. Finally, the adipose-specific deletion of *Fasn* sensitized animals towards adipose wasting, demonstrating that loss of DNL signaling primes the cachectic state. As such, our results reveal a previously unappreciated PTHrP-PTH1R-DNL signaling axis that drives cancer-associated cachexia and provides a promising target to ameliorate cachectic wasting in PDAC patients.

Cancer cachexia involves complex multi-organ metabolic crosstalk [10], with tumor cells sending and receiving multiple inputs from systemic paracrine/endocrine signaling networks. Several mechanisms have been identified to date to indicate how tumor cells communicate with the muscle to facilitate muscle wasting and catabolism, but few studies have identified mediators of direct tumor to adipocyte crosstalk as drivers of adipose tissue wasting and subsequent muscle wasting [28]. This is important clinically, as adipose tissue wasting precedes muscle wasting in PDAC patients and can occur up to 1.5 years prior to diagnosis [29]. Similar phenomena have been observed in other cancers as well [14, 30, 31]. Our adipocyte-specific deletion of *Pth1r* interestingly halted both adipose wasting and muscle wasting, suggesting that adipose wasting in this model may fuel muscle wasting. Future studies will seek to identify and functionally characterize how these adipose tissue-secreted signaling molecules, called “adipokines”, mediate muscle wasting, either through direct catabolism or by altering the metabolic status of the host.

Adipose tissue wasting during cancer cachexia has primarily been attributed to the induction of a UCP1-driven thermogenic program that promotes adipocyte browning [32].

358 Indeed, PTHrP is known to trigger adipose tissue browning in the Lewis Lung Carcinoma (LLC) model of cancer cachexia [6], and we find a modest induction of adipose UCP1 in
360 our PDAC-associated cachexia models (Figure 4D). However, we found a more profound downregulation of *de novo* lipogenesis in our system that suppresses lipid production in
362 adipocytes and primes them for cachectic wasting. Thus, harnessing new therapies to block or reverse the loss of DNL hold promise as a means to reverse cachectic wasting
364 of adipose tissue depots. One such approach that shows promise in preclinical models is the Peroxisome proliferator-activated receptor alpha (PPARα) agonist fenofibrate, which
366 has been shown to rescue reduced *Acly*, *Fasn*, *Acsl1*, and *Acsl5* in hepatic *de novo* lipogenesis, thus restoring lipid homeostasis in the liver and improving overall survival
368 [16]. Importantly, our data indicate that PPARα (encoded by *Ppara*) is still expressed, albeit at slightly lower levels, in the adipose of PTHrP tumor bearing animals, and thus its
370 reactivation is an attractive therapeutic target to pursue in future studies.

372 Prior correlative studies in a small cohort consisting of cachectic (weight losing) and non-cachectic (weight stable) patients suggested that enhanced adipocyte lipolysis, but *not*
374 reduced lipogenesis was involved in adipose tissue loss in cancer cachexia [33]. Provocatively, other work has demonstrated that whole body lipolytic rate in cancer
376 patients is not different from healthy controls, suggesting that the loss of body fat in cancer cachexia is due to reduced lipogenesis rather than augmented lipolysis [34]. The latter is
378 supported by clinical data to show that lipogenic enzymes such as FASN are reduced in adipose from cachectic patients [35, 36], consistent with our experiments showing that
380 PTHrP mediates loss of DNL in cachectic adipose tissue. Nonetheless, subsequent

functional studies in the field have primarily focused on the role of enhanced lipolysis, and not reduced DNL, in mediating adipose tissue loss. This work has confirmed that lipases are enriched in the cachectic state, which can be blocked through the inhibition of key lipases such as adipose triglyceride lipase (ATGL) or hormone-sensitive lipase (HSL) to limit adipose wasting [14]. Surprisingly, in PTHrP-driven adipose wasting, the expression of most cachexia-associated lipases, such as ATGL (*Pnpla2*), HSL (*Lipe*), and Monoglyceride Lipase (*Mgll*), were unchanged or even reduced in the cachectic state, suggesting that they are not driving the adipose tissue wasting phenotype in this model or that their regulation occurs post-transcriptionally. Rather, our work demonstrates that the loss of *de novo* lipogenesis, as opposed to the activation of lipases, in adipocytes primes the host for cachectic adipose tissue wasting. Consistent with this working model, prior work has demonstrated that the decrease in adipose tissue mass is due to reduced adipocyte size and not from a reduction in the total number of adipocytes (i.e. adipocyte death) [33, 37]. It is likely that the balance between adipose tissue lipolysis and lipogenesis is altered during progressive cachexia-associated adipose wasting, and thus different models may find varying functional roles for these enzymes during different stages of cachexia progression. Nonetheless, drugs targeting lipases and DNL components will need to achieve a balance to restore lipid homeostasis and block adipose wasting.

PDAC patients with higher serum levels of PTHrP lose significantly more weight, have reduced handgrip strength, and score lower on the Karnofsky Performance Status (KPS) scale relative to those with lower serum PTHrP, indicative of enhanced cachectic burden

404 [23]. Additionally, whole body fat oxidation is increased in PDAC patients with high PTHrP, suggesting a perturbed homeostasis between lipolysis and lipogenesis [23], in agreement
406 with our preclinical experiments in mice. Critically, in our models, disrupting direct tumor-to-adipocyte crosstalk by deleting *Pth1r* on adipocytes was sufficient to block cachectic
408 wasting, thereby setting the stage for PTHrP- or PTH1R-targeted therapeutic interventions such as the anti-PTHrP monoclonal antibody therapy that we used. This
410 result, combined with our prior work showing that PTHrP facilitates tumor growth and metastasis, demonstrates that blocking PTHrP-PTH1R signaling axis is a potent means
412 to block many of the confounding factors in PDAC that lead to its dismal overall survival rate. Interestingly, PTHrP/*PTHLH* is a squamous identity gene and is highly expressed in
414 many squamous carcinomas, including the squamous/basal-like subtype of PDAC [19], lung squamous cell carcinoma [38], head and neck squamous cell carcinoma [39], oral
416 squamous cell carcinoma [40], and cervical squamous cell carcinoma [41]. Many of these squamous cancers also have high levels of cancer-associated cachexia, suggesting that
418 targeting PTHrP in other cancers to block cachectic wasting warrants further preclinical testing. In a recent pan-cancer analysis, patients with high serum PTHrP levels lost ~7%
420 of their body weight independent of tumor burden, while those without PTHrP in their serum lost only ~1% [42], highlighting that PTHrP may also drive wasting in other cancers.
422 Notably, the Lewis lung cancer model of cancer cachexia was similarly responsive to anti-PTHrP therapy [6], perhaps pointing towards a more broadly applicable mechanism of
424 PTHrP-induced cachectic wasting across cancer types.

METHODS

426 ***Mice***

Kras$^{LSL\text{-}G12D}$; *Trp53*$^{LSL\text{-}R172H}$; *Pdx1-Cre*; *Rosa26*$^{LSL\text{-}YFP}$ (KPCY) and *Kras*$^{LSL\text{-}G12D}$; *Trp53*$^{LSL\text{-}}$
428 ^{R172H}; *Pdx1-Cre*; *Rosa26*$^{LSL\text{-}YFP}$; *Pthlh*$^{Loxp/wt}$ (KPCY-Pthlh^{Het}) mice have been described previously [18, 19]. *Pthlh*^{LoxP} mice were a generous gift from Dr. Andrew Karaplis (McGill
430 University) [43]. *Pth1r*^{LoxP} mice were a generous gift from Dr. Henry Kronenberg (Harvard University) [44]. Fasn^{LoxP} mice were generously provided by Dr. Clay Semenkovich
432 (Washington University at St. Louis) [45]. Adiponectin-Cre and wild-type C57BL/6J mice were purchased from the Jackson Laboratory (Stock # 028020 and #000664,
434 respectively). *Fasn*^{LoxP} or *Pthlh*^{LoxP} mice were crossed with Adiponectin-Cre mice to generate *Adiponectin-Cre; Fasn*$^{LoxP/LoxP}$ (Fasn$^{Adipo\text{-}cKO}$) and *Adiponectin-Cre; Pth1r*$^{LoxP/LoxP}$
436 (Pth1r$^{Adipo\text{-}cKO}$) lines, respectively. For survival analysis, mice were palpated for tumors and examined for evidence of morbidity twice weekly and sacrificed when moribund. Mice
438 treated with monoclonal neutralizing antibody against PTHrP (anti-PTHrP; generously provided by Dr. Richard Kremer, McGill University; 200µg/injection) or anti-IgG control
440 were injected three times per week every 48 hours for the indicated time. Mice were treated with rPTHrP (1mg/kg; Bachem T-4512) for 5 consecutive days, and tissues were
442 harvested within 1 hour of the final dosing. All vertebrate animals were maintained, and experiments were conducted in compliance with the NIH guidelines for animal research
444 and approved by the University of Massachusetts Chan Medical School Institutional Animal Care and Use Committee.

446

Genotyping

448 Mice were genotyped by automated genotyping services via TransnetYX for the following alleles: *Kras*$^{LSL\text{-}G12D}$, *Trp53*$^{LSL\text{-}R172H}$, *Pdx1-Cre*, *Rosa26*$^{LSL\text{-}YFP}$, *Pth1r*, *Adiponectin-Cre*,
450 and *Pthlh*^{Loxp}. For Fasn$^{Adipo\text{-}cKO}$ mice, conventional PCR genotyping reactions were performed. Briefly, tails were cut and immersed in lysis buffer (40% NaOH + 0.5M EDTA
452 pH 8) for one hour and incubated at 95°C, followed by addition of neutralization buffer (40mM Tris-HCl). PCR reactions were carried out with the following primers:
454 *Fasn forward: 5' - GGA TAG CTG TGT AGT GTA ACC AT -3'*
Fasn reverse: 5'- GGT CAT CGT GAT AAC CAC ACA T -3'
456 *Adipo-Cre transgene forward: 5'- ACG GAC AGA AGC ATT TTC CA -3'*
Adipo-Cre transgene reverse: 5'- GGA TGT GCC ATG TGA GTC TG - 3'
458 *Adipo-Cre internal control forward: 5'- CTA GGC CAC AGA ATT GAA AGA TCT -3'*
Adipo-Cre internal control reverse: 5'- GTA GGT GGA AAT TCT AGC ATC ATC C -3'
460

Orthotopic injection

462 Orthotopic injection was performed as previously described [46]. Briefly, C57BL/6 mice were anesthetized using isoflurane. A small incision was made on the upper left quadrant
464 of the mouse, and the pancreas was exteriorized on a sterile field. 1.0 x 10^5 cells were injected into the pancreas in 100ul sterile PBS via an insulin syringe. A cotton swab was
466 held over the site of injection. After injection, the pancreas was placed back into the peritoneal cavity and the incision was sutured with 4-0 Vicryl sutures. The mice received
468 meloxicam post-surgery and were monitored daily following surgery to assess post-surgery recovery. For each experiment, the sex of mice was matched to the sex of the
470 KPCY cell line.

472 ***Immunohistochemistry and immunofluorescence staining***

For staining of mouse tissues, zinc formalin-fixed paraffin embedded (FFPE) tissues were
474 dewaxed by baking in the oven at 60°C for an hour. Following dewaxing, tissues were rehydrated by serial immersions in xylene-substituent histoclear and ethanol gradients.
476 Antigen retrieval was performed using citric acid-based antigen retrieval buffer (Vector laboratories H-3300). Plin1 (Cell signaling technologies 9349), PTHrP (Sigma AV33885),
478 and PTH1R (Abcam ab189924) primary antibodies were used at 1:1000 dilution overnight at 4°C. Tissues were incubated with either HRP-tagged secondary antibody (Vector
480 laboratories MP-7401) or donkey anti-rabbit Alexa fluor 594 (Fisher Scientific Cat #A21207) at room temperature for 1 hour and followed with hematoxylin counterstain or
482 mounted with DAPI mounting media. Images were acquired on a Leica Thunder Imager or EVOS M5000.

484

Human specimens

486 Primary PDAC patient tumor samples and associated omental adipose tissues were obtained from decedents who had previously been diagnosed with pancreatic ductal
488 adenocarcinoma from the University of Nebraska Medical Center's Tissue Bank through the Rapid Autopsy Program (RAP) in compliance with IRB 091-01. Non-cancer tissues
490 are collected in a manner similar to RAP specimens through the UNMC Normal Organ Recovery (NORs) Program in association with LiveOn Nebraska. To ensure specimen
492 quality, organs were harvested within three hours post-mortem and the specimens flash frozen in liquid nitrogen or placed in formalin for immediate fixation. Sections were cut

494 from paraffin blocks of formalin fixed tissue into 4-micron thick sections and mounted on charged slides. Pancreatic cancer patients with a known history of body weight loss, as
496 confirmed by the pathologist, were binned into cachectic and non-cachectic cohorts. The primary tumors were processed and stained for PTHrP immunohistochemistry as
498 described above. The slides were scanned by the UMass Chan SCOPE core facility using a SL Slide Scanner, followed by PTHrP H Score quantification using QuPath software.

500

Cell lines and culture conditions

502 Murine PDAC cell lines were derived from KPCY mice that were backcrossed onto the C57BL/6J strain [47]. KPCY-EV and KPCY-PTHrP^{OE} cells were described previously [19].
504 All cell lines were maintained in Dulbecco's modified eagle medium (DMEM) with 10% fetal bovine serum (FBS) and 1% penicillin/streptomycin (P/S) at 5% CO_2 at 37°C. Cell
506 lines were tested regularly for *Mycoplasma*.

508 ***Cell proliferation assay***

The WST-1 cell proliferation assay (ab65475, Abcam) was performed per the
510 manufacturer's instructions. Briefly, 2.0×10^3 cells were plated on 96-well plates and grown in DMEM supplemented with 10% FBS and 1% P/S. Fresh media containing 10%
512 WST solution was incubated on the cells for 2 hours at 37°C. After shaking the plate, the absorbance was read at 420 to 480 nm with a reference wavelength of 650 nm. Final
514 absorbance was obtained by subtracting the 650-nm reference wavelength from the 420- to 480-nm read.

516

Western blot analysis

518 Inguinal white adipose tissues were snap-frozen in liquid nitrogen immediately after retrieving from orthotopic and GEM mice. The iWAT's were transferred to 2ml Eppendorf
520 tubes with pre-cooled metal bead and homogenized using Cryomill (Retsch) for 3 minutes to get a fine powder. The powderized iWAT's were then lysed in RIPA buffer containing
522 protease and phosphatase inhibitors (Sigma 04693124001 and Roche 04906837001). The samples were centrifuged at 15,000 g for 15 min at 4°C, and the supernatant was
524 collected for western blotting. Lysates were run on NuPAGE gels (Thermo Fisher NP0336BOX), transferred to PVDF membranes, and stained with primary antibodies:
526 Fasn (Cell signaling technologies 3180), Acly (Proteintech 15421-1-1 AP), Acaca (Cell signaling technologies 3662) and beta-actin (Sigma A5316). Membranes were washed
528 and stained with secondary antibodies: donkey anti-mouse IgG IRDye 800 (LICORbio 926-32212) or donkey anti-rabbit IgG IRDye 800 (LICORbio 926-32213) or donkey anti-
530 rabbit IgG IRDye 680 (LICORbio 926-68073) (1:15,000), washed, and imaged on a LI-COR Odyssey imaging system.

532

RNA extraction and qPCR

534 RNA was extracted from cryomilled adipose tissues using QIAzol/chloroform and Qiagen RNeasy kit (Cat #74106) following the manufacturer's protocol. For extracting RNA from
536 the iWAT, powderized tissues were resuspended in 1ml QIAzol per sample and lysed using TissueLyser II (Qiagen Cat#) and pre-cooled metal beads. The lysed sample was
538 mixed with chloroform and mixed vigorously, followed by centrifugation at 4°C for 10 minutes at 10,000g. The upper aqueous phase was mixed with 70% ethanol in 1:1 ratio

540 and transferred to the RNA spin columns from the Qiagen RNeasy kit and spun for 20 seconds at 9000g. All the remaining steps were followed as per manufacturer's
542 guidelines. Extracted RNA was quantified using Nanodrop and cDNA was prepared using 100ng-1000ng RNA using the New England Biolabs LunaScript RT supermix (Cat#
544 M3010L). Quantitative PCR was setup using Luna Universal qPCR Master Mix (Cat #M3003E). The following primers were used:

546 *Pth1r forward: 5'- TCT GCA ATG GTG AGG TGC AG - 3'*

Pth1r reverse: 5'- GCT ACT CCC ACT TCG TGC TT - 3'

548 *Fasn forward: 5'- GGA GGT GGT GAT AGC CGG TAT - 3'*

Fasn reverse: 5'- TGG GTA ATC CAT AGA GCC CAG - 3'

550 *Acly forward: 5'- ACC CTT TCA CTG GGG ATC ACA -3'*

Acly reverse: 5'- GAC AGG GAT CAG GTA TTC CTT G - 3'

552 *Acaca forward: 5'- ATT GTG GCT CAA ACT GCA GGT - 3'*

Acaca reverse: 5'- GCC AAT CCA CTC GAA GAC CA -3'

554 *Murf1 forward: 5'- GGA CGG AAA TGC TAT GGA GAA CC CC-3'*

Murf1 reverse: 5'- GAT GGC TGT TTC CAC AAG CTT GG - 3'

556 *Atrogin1 forward: 5'- CCT CAG CAG TTA CTG CAA CAA GGA -3'*

Atrogin 1 reverse: 5'- CAT CTT CTT CCA ATC CAG CTG C - 3'

558 *Chrebp-a forward: 5'- CGA CAC TCA CCC ACC TCT TC -3'*

Chrebp-a reverse: 5' - TTG TTC AGC CGG ATC TTG TC - 3'

560 *Chrebp-b forward: 5' - TCT GCA GAT CGC GTG GAG -3'*

Chrebp-b reverse: 5'- CTT GTC CCG GCA TAG CAA C -3'

562 *Srebf1c forward: 5'- AAG CAA ATC ACT GAA GGA CCT GG - 3'*

Srebf1c reverse: 5'- AAA GAC AAG CTA CTC TGG GAG -3'

564 *18S RNA forward: 5'- CGA ACG TCT GCC CTA TCA ACT T - 3'*

18S RNA reverse: 5'- CCG GAA TCG AAC CCT GAT T - 3'

566

RNA-seq library prep and GSEA

568 Frozen iWAT tissues were cryomilled and RNA was isolated using Qiazol and Qiagen RNAeasy mini kits. A quantity of 500ng total RNA was used for poly(A) mRNA purification 570 using the NEBNext poly(A) mRNA magnetic isolation module (E7490L). Libraries were prepared using the NEBNext Ultra II Directional Library Prep Kit for Illumina (E7760L) as 572 per the manufacturer's recommendations and were barcoded using NEBNext Multiplex Oligos for Illumina (Dual Index Primers set 2 E7780S) during PCR amplification. Final 574 libraries were quantified using the NEBNext Library Quant Kit for Illumina (E7630L). Sequencing was performed using an Illumina NextSeq2000 with 115 bp single-end reads, 576 plus 8 cycles for barcodes. Fastq files were generated with Illumina DRAGEN BCL Convert v3.8.4. Heatmaps were generated by Morpheus (Broad Institute).

578

The RNA-seq analysis was performed using OneStopRNAseq [48]. Briefly, FastQC and 580 MultiQC were used for raw reads quality control and QoRTs for post-alignment quality control [49, 50]. Reads were aligned to the reference genome assembly mm10 with 582 star_2.7.5a and annotated with gencode.vM25.primary_assembly [51, 52]. Aligned exon reads were counted toward gene expression with featureCounts_2.0.0 with default 584 settings [53]. Differential expression (DE) analysis was performed with DESeq2_1.28.1 [54]. Significantly differentially expressed genes (DEGs) were filtered with the criteria FDR

586 < 0.05 (|LFC|) > 0.585. Gene set enrichment analysis were performed with GSEA [55]. Heatmaps of TPM values were generated by Morpheus (Broad Institute).

588

Adipocyte size quantification

590 Inguinal white adipose tissues were harvested, sectioned, and stained with hematoxylin and eosin. H&E stained tissues were imaged at 20X magnification and adipocyte size

592 (area in μm^2) was quantified using Adiposoft plugin in ImageJ software [56]. All of the adipocyte areas counted by Adiposoft were included in the analysis and are represented

594 as relative frequencies.

596 ***Lentiviral transduction***

KPCY-PTHrP^{OE} cells were previously generated by lentiviral-mediated overexpression of

598 *Pthlh* [19]. Briefly, KPCY cells were transduced with pLenti-C-Myc-DDK-P2A-Puro Lentiviral Particles with EV (Origene PS100092) or Pthlh ORF (Origene MR201519L3)

600 and stably selected with puromycin (8 µg/ml). Stable KPCY-PTHrP^{OE} cells were maintained with puromycin after selection.

602

Statistical analysis

604 All data points are biological replicates and represent individual mice, tissues, or cell samples. The data was first tested for normal distribution, followed by the appropriate

606 statistical test as indicated in the figure legends. Data are represented as mean ± standard deviation; *$P<0.05$; non-significant P values are indicated in the figure text or

608 legend. All statistical analysis was performed using GraphPad Prism.

610 ***Data and code availability***

All sequencing data have been deposited in the Gene Expression Omnibus under the

612 series GSE298308.

614

ACKNOWLEDGEMENTS

616 This work was supported by an American Gastroenterology Association Bern Schwartz Research Scholar Award in Pancreatic Cancer (JRP); National Institute of Health (NIH) 618 K99-R00 CA252153 (JRP); US Department of Defense (DOD) Pancreatic Cancer Research Program (PCARP) Idea Development Award PA230161P1 (JRP and DG); 620 Hopper-Belmont Inspiration Award (NB); Pancreatic Cancer Alliance (PCA) Postdoctoral Fellowship (NB); NIH Innate Immunity Training Program T32 AI095213 (JP); NIH Institute 622 for Maximizing Student Development T32 GM135751 (CJ); Canadian Institutes of Health Research (CIHR) MOP142287 (RK); Pancreatic Cancer Detection Consortium, 624 U01CA210240; NCI Cancer Center Support Grant, P30CA36727; NCI Research Specialist, R50CA211462; NIH DK130852 (MPC); Breast Cancer Alliance Young 626 Investigator Grant (EVW); Massachusetts Life Sciences Center Bits to Bytes grant (to Drs. Dori Schafter and Christina Baer); and Massachusetts Life Sciences Center 628 Research Infrastructure grant (to Drs. Kate Fitzgerald and Christina Baer). We acknowledge and thank the Sanderson Center for Optical Experimentation (SCOPE; Dr. 630 Christina Baer and Jill McConnell) and Morphology core facilities at the University of Massachusetts Chan Medical School; and Pancreatic Cancer Mouse Hospital and the 632 Molecular Pathology and Imaging Core at the University of Pennsylvania.

634 RK is the inventor of the therapeutic monoclonal anti-PTHrP antibodies used in this study and authorized for use by Miramab Bioscience. RK holds an equity stake in 636 Miramab Bioscience.

REFERENCES

638 1. Siegel, R.L., A.N. Giaquinto, and A. Jemal, *Cancer statistics, 2024.* CA Cancer J Clin, 2024. **74**(1): p. 12-49.

640 2. *American Cancer Society: Cancer Facts & Figures 2025.* Atlanta: American Cancer Society, 2025

642 3. Baracos, V.E., L. Martin, M. Korc, D.C. Guttridge, and K.C.H. Fearon, *Cancer-associated cachexia.* Nat Rev Dis Primers, 2018. **4**: p. 17105.

644 4. Henderson, S.E., N. Makhijani, and T.A. Mace, *Pancreatic Cancer-Induced Cachexia and Relevant Mouse Models.* Pancreas, 2018. **47**(8): p. 937-945.

646 5. Narsale, A.A. and J.A. Carson, *Role of interleukin-6 in cachexia: therapeutic implications.* Curr Opin Support Palliat Care, 2014. **8**(4): p. 321-7.

648 6. Kir, S., J.P. White, S. Kleiner, L. Kazak, P. Cohen, et al., *Tumour-derived PTH-related protein triggers adipose tissue browning and cancer cachexia.* Nature, 2014. **513**(7516): p. 100-4.

650 7. Patel, H.J. and B.M. Patel, *TNF-alpha and cancer cachexia: Molecular insights and clinical implications.* Life Sci, 2017. **170**: p. 56-63.

652 8. Ling, T., J. Zhang, F. Ding, and L. Ma, *Role of growth differentiation factor 15 in cancer cachexia (Review).* Oncol Lett, 2023. **26**(5): p. 462.

654 9. Groarke, J.D., J. Crawford, S.M. Collins, S. Lubaczewski, E.J. Roeland, et al., *Ponsegromab for the Treatment of Cancer Cachexia.* N Engl J Med, 2024. **391**(24): p. 2291-2303.

656 10. Ferrer, M., T.G. Anthony, J.S. Ayres, G. Biffi, J.C. Brown, et al., *Cachexia: A systemic consequence of progressive, unresolved disease.* Cell, 2023. **186**(9): p. 1824-1845.

658 11. Fearon, K., F. Strasser, S.D. Anker, I. Bosaeus, E. Bruera, et al., *Definition and classification of cancer cachexia: an international consensus.* Lancet Oncol, 2011. **12**(5): p. 489-95.

660 12. Weber, B.Z.C., D.H. Arabaci, and S. Kir, *Metabolic Reprogramming in Adipose Tissue During Cancer Cachexia.* Front Oncol, 2022. **12**: p. 848394.

662 13. Petruzzelli, M., M. Schweiger, R. Schreiber, R. Campos-Olivas, M. Tsoli, et al., *A switch from white to brown fat increases energy expenditure in cancer-associated cachexia.* Cell
664 Metab, 2014. **20**(3): p. 433-47.

14. Das, S.K., S. Eder, S. Schauer, C. Diwoky, H. Temmel, et al., *Adipose triglyceride lipase*
666 *contributes to cancer-associated cachexia.* Science, 2011. **333**(6039): p. 233-8.

15. Fearon, K.C., D.J. Glass, and D.C. Guttridge, *Cancer cachexia: mediators, signaling, and*
668 *metabolic pathways.* Cell Metab, 2012. **16**(2): p. 153-66.

16. Yang, X., J. Wang, C.Y. Chang, F. Zhou, J. Liu, et al., *Leukemia inhibitory factor suppresses*
670 *hepatic de novo lipogenesis and induces cachexia in mice.* Nat Commun, 2024. **15**(1): p. 627.

672 17. Hingorani, S.R., L. Wang, A.S. Multani, C. Combs, T.B. Deramaudt, et al., *Trp53R172H and KrasG12D cooperate to promote chromosomal instability and widely metastatic*
674 *pancreatic ductal adenocarcinoma in mice.* Cancer Cell, 2005. **7**(5): p. 469-83.

18. Rhim, A.D., E.T. Mirek, N.M. Aiello, A. Maitra, J.M. Bailey, et al., *EMT and dissemination*
676 *precede pancreatic tumor formation.* Cell, 2012. **148**(1-2): p. 349-61.

19. Pitarresi, J.R., R.J. Norgard, A.M. Chiarella, K. Suzuki, B. Bakir, et al., *PTHrP Drives*
678 *Pancreatic Cancer Growth and Metastasis and Reveals a New Therapeutic Vulnerability.* Cancer Discov, 2021. **11**(7): p. 1774-1791.

680 20. Gumucio, J.P. and C.L. Mendias, *Atrogin-1, MuRF-1, and sarcopenia.* Endocrine, 2013. **43**(1): p. 12-21.
682 21. Rupert, J.E., A. Narasimhan, D.H.A. Jengelley, Y. Jiang, J. Liu, et al., *Tumor-derived IL-6 and trans-signaling among tumor, fat, and muscle mediate pancreatic cancer cachexia.* J Exp
684 Med, 2021. **218**(6).
22. Goncalves, M.D., S.K. Hwang, C. Pauli, C.J. Murphy, Z. Cheng, et al., *Fenofibrate prevents*
686 *skeletal muscle loss in mice with lung cancer.* Proc Natl Acad Sci U S A, 2018. **115**(4): p. E743-E752.
688 23. Iresjo, B.M., S. Kir, and K. Lundholm, *Parathyroid hormone related protein (PTHrP) in patients with pancreatic carcinoma and overt signs of disease progression and host tissue*
690 *wasting.* Transl Oncol, 2023. **36**: p. 101752.
24. Urena, P., X.F. Kong, A.B. Abou-Samra, H. Juppner, H.M. Kronenberg, et al., *Parathyroid*
692 *hormone (PTH)/PTH-related peptide receptor messenger ribonucleic acids are widely distributed in rat tissues.* Endocrinology, 1993. **133**(2): p. 617-23.
694 25. Emont, M.P., C. Jacobs, A.L. Essene, D. Pant, D. Tenen, et al., *A single-cell atlas of human and mouse white adipose tissue.* Nature, 2022. **603**(7903): p. 926-933.
696 26. De Miguel, F., P. Martinez-Fernandez, C. Guillen, A. Valin, A. Rodrigo, et al., *Parathyroid hormone-related protein (107-139) stimulates interleukin-6 expression in human*
698 *osteoblastic cells.* J Am Soc Nephrol, 1999. **10**(4): p. 796-803.
27. Tuca, A., P. Jimenez-Fonseca, and P. Gascon, *Clinical evaluation and optimal management*
700 *of cancer cachexia.* Crit Rev Oncol Hematol, 2013. **88**(3): p. 625-36.
28. Schmidt, S.F., M. Rohm, S. Herzig, and M. Berriel Diaz, *Cancer Cachexia: More Than*
702 *Skeletal Muscle Wasting.* Trends Cancer, 2018. **4**(12): p. 849-860.
29. Sah, R.P., A. Sharma, S. Nagpal, S.H. Patlolla, A. Sharma, et al., *Phases of Metabolic and*
704 *Soft Tissue Changes in Months Preceding a Diagnosis of Pancreatic Ductal Adenocarcinoma.* Gastroenterology, 2019. **156**(6): p. 1742-1752.
706 30. Rohm, M., M. Schafer, V. Laurent, B.E. Ustunel, K. Niopek, et al., *An AMP-activated protein kinase-stabilizing peptide ameliorates adipose tissue wasting in cancer cachexia in mice.*
708 Nat Med, 2016. **22**(10): p. 1120-1130.
31. Agustsson, T., M. Ryden, J. Hoffstedt, V. van Harmelen, A. Dicker, et al., *Mechanism of*
710 *increased lipolysis in cancer cachexia.* Cancer Res, 2007. **67**(11): p. 5531-7.
32. Kir, S. and B.M. Spiegelman, *Cachexia & Brown Fat: A Burning Issue in Cancer.* Trends
712 Cancer, 2016. **2**(9): p. 461-463.
33. Ryden, M., T. Agustsson, J. Laurencikiene, T. Britton, E. Sjolin, et al., *Lipolysis--not*
714 *inflammation, cell death, or lipogenesis--is involved in adipose tissue loss in cancer cachexia.* Cancer, 2008. **113**(7): p. 1695-704.
716 34. Jeevanandam, M., G.D. Horowitz, S.F. Lowry, and M.F. Brennan, *Cancer cachexia and the rate of whole body lipolysis in man.* Metabolism, 1986. **35**(4): p. 304-10.
718 35. Notarnicola, M., A. Miccolis, V. Tutino, D. Lorusso, and M.G. Caruso, *Low levels of lipogenic enzymes in peritumoral adipose tissue of colorectal cancer patients.* Lipids, 2012. **47**(1): p.
720 59-63.
36. Fang, R., L. Yan, and Z. Liao, *Abnormal lipid metabolism in cancer-associated cachexia and*
722 *potential therapy strategy.* Front Oncol, 2023. **13**: p. 1123567.

37. Bing, C., S. Russell, E. Becket, M. Pope, M.J. Tisdale, et al., *Adipose atrophy in cancer cachexia: morphologic and molecular analysis of adipose tissue in tumour-bearing mice.* Br J Cancer, 2006. **95**(8): p. 1028-37.
38. Hastings, R.H., F. Araiza, D.W. Burton, and L.J. Deftos, *Role of parathyroid hormone-related protein in lung cancer cell survival.* Chest, 2004. **125**(5 Suppl): p. 150S.
39. Chang, W.M., Y.F. Lin, C.Y. Su, H.Y. Peng, Y.C. Chang, et al., *Parathyroid Hormone-Like Hormone is a Poor Prognosis Marker of Head and Neck Cancer and Promotes Cell Growth via RUNX2 Regulation.* Sci Rep, 2017. **7**: p. 41131.
40. Lv, Z., X. Wu, W. Cao, Z. Shen, L. Wang, et al., *Parathyroid hormone-related protein serves as a prognostic indicator in oral squamous cell carcinoma.* J Exp Clin Cancer Res, 2014. **33**(1): p. 100.
41. Kitazawa, S., R. Kitazawa, M. Fukase, T. Fujimori, and S. Maeda, *Immunohistochemical evaluation of parathyroid hormone-related protein (PTHrP) in the uterine cervix.* Int J Cancer, 1992. **50**(5): p. 731-5.
42. Hong, N., H.J. Yoon, Y.H. Lee, H.R. Kim, B.W. Lee, et al., *Serum PTHrP Predicts Weight Loss in Cancer Patients Independent of Hypercalcemia, Inflammation, and Tumor Burden.* J Clin Endocrinol Metab, 2016. **101**(3): p. 1207-14.
43. He, B., R.A. Deckelbaum, D. Miao, M.L. Lipman, M. Pollak, et al., *Tissue-specific targeting of the pthrp gene: the generation of mice with floxed alleles.* Endocrinology, 2001. **142**(5): p. 2070-7.
44. Kobayashi, T., U.I. Chung, E. Schipani, M. Starbuck, G. Karsenty, et al., *PTHrP and Indian hedgehog control differentiation of growth plate chondrocytes at multiple steps.* Development, 2002. **129**(12): p. 2977-86.
45. Chakravarthy, M.V., Z. Pan, Y. Zhu, K. Tordjman, J.G. Schneider, et al., *"New" hepatic fat activates PPARalpha to maintain glucose, lipid, and cholesterol homeostasis.* Cell Metab, 2005. **1**(5): p. 309-22.
46. Aiello, N.M., A.D. Rhim, and B.Z. Stanger, *Orthotopic Injection of Pancreatic Cancer Cells.* Cold Spring Harb Protoc, 2016. **2016**(1): p. pdb prot078360.
47. Li, J., K.T. Byrne, F. Yan, T. Yamazoe, Z. Chen, et al., *Tumor Cell-Intrinsic Factors Underlie Heterogeneity of Immune Cell Infiltration and Response to Immunotherapy.* Immunity, 2018. **49**(1): p. 178-193 e7.
48. Li, R., K. Hu, H. Liu, M.R. Green, and L.J. Zhu, *OneStopRNAseq: A Web Application for Comprehensive and Efficient Analyses of RNA-Seq Data.* Genes (Basel), 2020. **11**(10).
49. Ewels, P., M. Magnusson, S. Lundin, and M. Kaller, *MultiQC: summarize analysis results for multiple tools and samples in a single report.* Bioinformatics, 2016. **32**(19): p. 3047-8.
50. Hartley, S.W. and J.C. Mullikin, *QoRTs: a comprehensive toolset for quality control and data processing of RNA-Seq experiments.* BMC Bioinformatics, 2015. **16**(1): p. 224.
51. Dobin, A., C.A. Davis, F. Schlesinger, J. Drenkow, C. Zaleski, et al., *STAR: ultrafast universal RNA-seq aligner.* Bioinformatics, 2013. **29**(1): p. 15-21.
52. Harrow, J., A. Frankish, J.M. Gonzalez, E. Tapanari, M. Diekhans, et al., *GENCODE: the reference human genome annotation for The ENCODE Project.* Genome Res, 2012. **22**(9): p. 1760-74.
53. Liao, Y., G.K. Smyth, and W. Shi, *featureCounts: an efficient general purpose program for assigning sequence reads to genomic features.* Bioinformatics, 2014. **30**(7): p. 923-30.

54. Love, M.I., W. Huber, and S. Anders, *Moderated estimation of fold change and dispersion for RNA-seq data with DESeq2.* Genome Biol, 2014. **15**(12): p. 550.
55. Subramanian, A., P. Tamayo, V.K. Mootha, S. Mukherjee, B.L. Ebert, et al., *Gene set enrichment analysis: a knowledge-based approach for interpreting genome-wide expression profiles.* Proc Natl Acad Sci U S A, 2005. **102**(43): p. 15545-50.
56. Galarraga, M., J. Campion, A. Munoz-Barrutia, N. Boque, H. Moreno, et al., *Adiposoft: automated software for the analysis of white adipose tissue cellularity in histological sections.* J Lipid Res, 2012. **53**(12): p. 2791-6.

FIGURE LEGENDS

778

Figure 1.

780 **(A)** Kaplan–Meier overall survival plots of KPCY and KPCY-Pthlh^{HET} mice. Log-rank $P <$ 0.0001. **(B)** Percent change from baseline bodyweight in KPCY and KPCY-Pthlh^{HET} mice.
782 **(C)** Carcass weights at endpoint from (B). **(D-F)** Representative H&E images and quantification of normalized tissue masses for iWAT **(D)**, eWAT **(E)**, and quads **(F)** from
784 non-tumor bearing (NTB), KPCY, and KPCY-Pthlh^{HET} mice at endpoint. Scale bars, 100 µm. **(G-I)** Representative H&E images and quantification of normalized tissue masses for
786 iWAT **(G)**, eWAT **(H)**, and quads **(I)** from NTB, KPCY, and KPCY-Pthlh^{HET} mice at a set endpoint of 5 months of age. Scale bars, 100 µm. **(J)** Histograms of adipocyte size in
788 iWAT from NTB, KPCY, and KPCY-Pthlh^{HET} mice. **(K)** Immunofluorescence staining of PLIN1 in iWAT from NTB, KPCY, and KPCY-Pthlh^{HET} mice. Scale bars, 50 µm. **(L)**
790 Representative images and H Score quantification of PTHrP IHC in primary tumors from cachectic (N=21) and non-cachectic (N=22) PDAC patients. Scale bars, 100 µm.
792 Statistical analysis by Mann–Whitney *U* test (B, C, and D) or Student unpaired *t* test (D, E, F, G, H, I and L), with significance indicated (*, $P < 0.05$). Error bars indicate standard
794 deviation (SD).

796

Figure 2.

798 **(A)** Kaplan–Meier overall survival plots of C57BL/6 mice orthotopically implanted with KPCY-EV (N=9) or KPCY-PTHrP^{OE} (N=8) cells. Log-rank $P < 0.0001$. **(B)** Representative
800 dissection images of iWAT from KPCY-EV or KPCY-PTHrP^{OE} orthotopic tumor-bearing mice. Scale bars, 1 cm. **(C-D)** Representative H&E images and quantification of
802 normalized tissue masses for iWAT from KPCY-EV or KPCY-PTHrP^{OE} orthotopic tumor-bearing mice. Scale bars, 100 µm. **(E)** Histograms of adipocyte size in iWAT from KPCY-
804 EV or KPCY-PTHrP^{OE} orthotopic tumor-bearing mice. **(F)** Immunofluorescence staining of PLIN1 in iWAT from KPCY-EV or KPCY-PTHrP^{OE} orthotopic tumor-bearing mice. Scale
806 bars, 50 µm. **(G-H)** Representative H&E images and quantification of normalized tissue masses for quads from KPCY-EV or KPCY-PTHrP^{OE} orthotopic tumor-bearing mice.
808 Scale bars, 100 µm. **(I-J)** Schematic depicting rPTHrP treatment once per day over five days and quantification of normalized tissue masses of iWAT from rPTHrP- or sham-
810 injected C57BL/6 mice. Representative Statistical analysis by Student unpaired *t* test (D and H) with significance indicated (*, $P < 0.05$). Error bars indicate standard deviation
812 (SD).

814 **Figure 3.**

(A) Human *PTH1R* expression from the GTEX database in the indicated tissues. Adipose
816 and muscle tissues are highlighted. **(B)** qPCR for murine *Pth1r* expression in the indicated tissues; inguinal Brown Adipose Tissue (iBAT), subcutaneous Brown Adipose Tissue
818 (sBAT). Adipose and muscle tissues are highlighted. **(C)** Single-cell RNA-seq clustering plots (left) and *PTH1R* expression (right) from the Emont *et al*., human adipocyte single
820 cell atlas [25]. **(D)** Immunofluorescence staining of PTH1R in iWAT from non-tumor bearing or KPCY mice. Scale bars, 100 µm. **(E-F)** H&E images and quantification of
822 normalized tissue masses for iWAT from KPCY-EV or KPCY-PTHrP^{OE} orthotopic tumor-

bearing mice with the indicated host genotypes. Scale bars, 100 μm. **(G)** Histograms of adipocyte size in iWAT from KPCY-PTHrP^{OE} orthotopic tumor-bearing WT or *Pth1r*$^{Adipo-cKO}$ host mice. **(H)** Immunofluorescence staining of PLIN1 in iWAT from KPCY-PTHrP^{OE} orthotopic tumor-bearing WT or *Pth1r*$^{Adipo-cKO}$ host mice. Scale bars, 50 μm. **(I-J)** H&E images and quantification of normalized tissue masses for quads from KPCY-EV or KPCY-PTHrP^{OE} orthotopic tumor-bearing mice with the indicated host genotypes. Scale bars, 100 μm. Statistical analysis by Student unpaired *t* test (F and J), with significance indicated (*, $P < 0.05$). Error bars indicate standard deviation (SD).

Figure 4.

(A) Volcano plot of differentially expressed genes from RNA-seq of iWAT from KPCY-EV or KPCY-PTHrP^{OE} orthotopic tumor-bearing mice in C57BL/6 hosts; DNL genes highlighted in blue. **(B)** Significantly altered gene set enrichment pathways enriched in iWAT from KPCY-EV (blue) or KPCY-PTHrP^{OE} (red) tumor-bearing animals. **(C)** GSEA plots of iWAT from KPCY-EV (blue) or KPCY-PTHrP^{OE} (red) tumor-bearing animals. **(D)** Heatmap of altered genes in the DNL, Lipase, Fatty Acid (FA) metabolism, TNF, and IL-6 pathways. **(E)** Schematic representation of the DNL pathway with red arrows indicating all downregulated genes in adipose from KPCY-PTHrP^{OE} tumor-bearing animals relative to KPCY-EV tumor-bearing animals. Created in BioRender. Pitarresi, J. (2025) https://BioRender.com/vapcw88

Figure 5.

(A) qPCR of *Ascc2*, *Acly*, *Acaca*, and *Fasn* in iWAT from KPCY-EV or KPCY-PTHrP^{OE} orthotopic tumor-bearing hosts. **(B)** Western blot analysis of FASN, ACACA, ACLY, and ACTIN in iWAT from KPCY-EV or KPCY-PTHrP^{OE} orthotopic tumor-bearing hosts. **(C)** qPCR of *Chrebp-a*, *Chrebp-b*, and *Srebf1c* in iWAT from KPCY-EV or KPCY-PTHrP^{OE} orthotopic tumor-bearing hosts. **(D-E)** Representative H&E images and quantification of normalized tissue masses for iWAT from KPCY-EV orthotopic tumor-bearing C57BL/6 or *Fasn*$^{Adipo-cKO}$ hosts. Scale bars, 100 μm. **(F)** Histograms of adipocyte size in iWAT from KPCY-EV orthotopic tumor-bearing C57BL/6 or *Fasn*$^{Adipo-cKO}$ hosts. **(G)** Immunofluorescence staining of PLIN1 in iWAT from KPCY-EV orthotopic tumor-bearing C57BL/6 or *Fasn*$^{Adipo-cKO}$ hosts. Scale bars, 50 μm. Statistical analysis by Student unpaired *t* test (A, C, and E), with significance indicated (*, $P < 0.05$). Error bars indicate standard deviation (SD).

Figure 6.

(A-B) Representative H&E images and quantification of normalized tissue masses for iWAT from anti-IgG or anti-PTHrP treated KPCY mice. Scale bars, 100 μm. **(C)** Histograms of adipocyte size in iWAT from anti-IgG or anti-PTHrP treated KPCY mice. **(D-E)** Representative H&E images and quantification of normalized tissue masses for quads from anti-IgG or anti-PTHrP treated KPCY mice. Scale bars, 100 μm. **(F-G)** Representative H&E images and quantification of normalized tissue masses for iWAT from anti-IgG or anti-PTHrP treated C57BL/6 mice orthotopically implanted with KPCY cells. Scale bars, 100 μm. **(H)** Histograms of adipocyte size in iWAT from anti-IgG or anti-PTHrP treated C57BL/6 mice orthotopically implanted with KPCY cells. **(I-J)** Representative H&E images and quantification of normalized tissue masses for quads

from anti-IgG or anti-PTHrP treated C57BL/6 mice orthotopically implanted with KPCY cells. Scale bars, 100 μm. **(K-L)** Immunofluorescence staining of PLIN1 in iWAT from KPCY mice treated with anti-IgG or anti-PthrP (K) or C57BL/6 mice orthotopically implanted with KPCY cells and treated with anti-IgG or anti-PTHrP (L). Scale bars, 50 μm. **(M)** GSEA plots of iWAT from animals orthotopically implanted with KPCY cells and treated with anti-PTHrP (red) or anti-IgG (blue) tumor-bearing animals. **(N)** qPCR of *Fasn* in iWAT from KPCY orthotopic tumor-bearing hosts treated with anti-IgG or anti-PTHrP therapy. Scale bars, 50 μm. Statistical analysis by Student unpaired *t* test (B, E, G, J, and N), with significance indicated (*, $P < 0.05$). Error bars indicate standard deviation (SD).

Figure 7.

Schematic of PTHrP-induced adipose tissue wasting. Tumor-derived PTHrP binds to PTH1R on adipocytes, which downregulates *de novo* lipogenesis in adipose tissue to facilitate wasting. Created in BioRender. Pitarresi, J. (2025) https://BioRender.com/wbw5raq

FIGURE 1

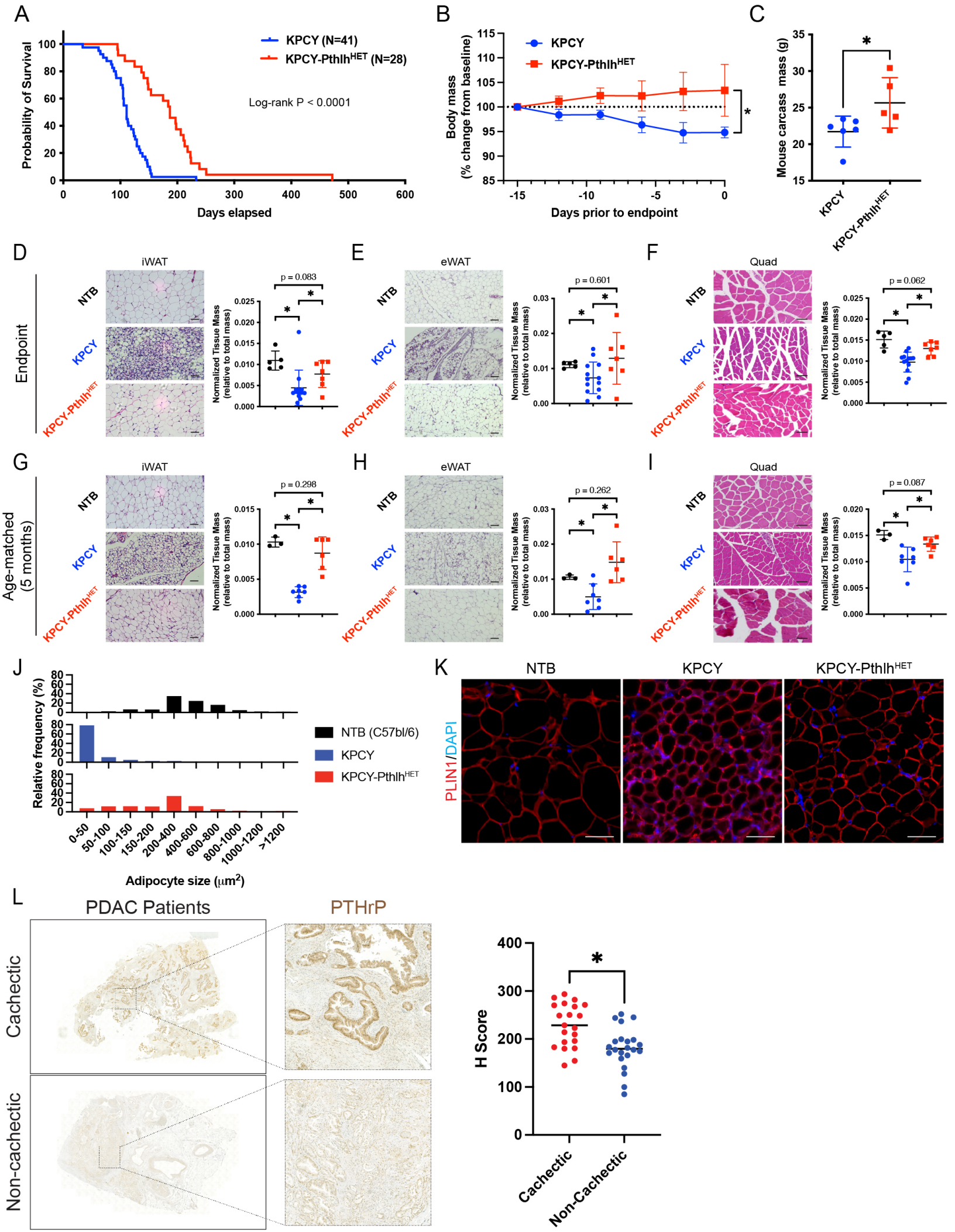
A
Probability of Survival
Days elapsed
KPCY (N=41)
KPCY-PthlhHET (N=28)
Log-rank P < 0.0001
B
Body mass (% change from baseline)
Days prior to endpoint
KPCY
KPCY-PthlhHET
C
Mouse carcass mass (g)
KPCY
KPCY-PthlhHET
D
iWAT
Endpoint
NTB
KPCY
KPCY-PthlhHET
Normalized Tissue Mass (relative to total mass)
p = 0.083
E
eWAT
p = 0.601
F
Quad
p = 0.062
G
iWAT
Age-matched (5 months)
p = 0.298
H
eWAT
p = 0.262
I
Quad
p = 0.087
J
Relative frequency (%)
NTB (C57bl/6)
KPCY
KPCY-PthlhHET
0-50
50-100
100-150
150-200
200-400
400-600
600-800
800-1000
1000-1200
>1200
Adipocyte size (μm2)
K
NTB
KPCY
KPCY-PthlhHET
PLIN1/DAPI
L
PDAC Patients
PTHrP
Cachectic
Non-cachectic
H Score
Cachectic
Non-Cachectic

FIGURE 2

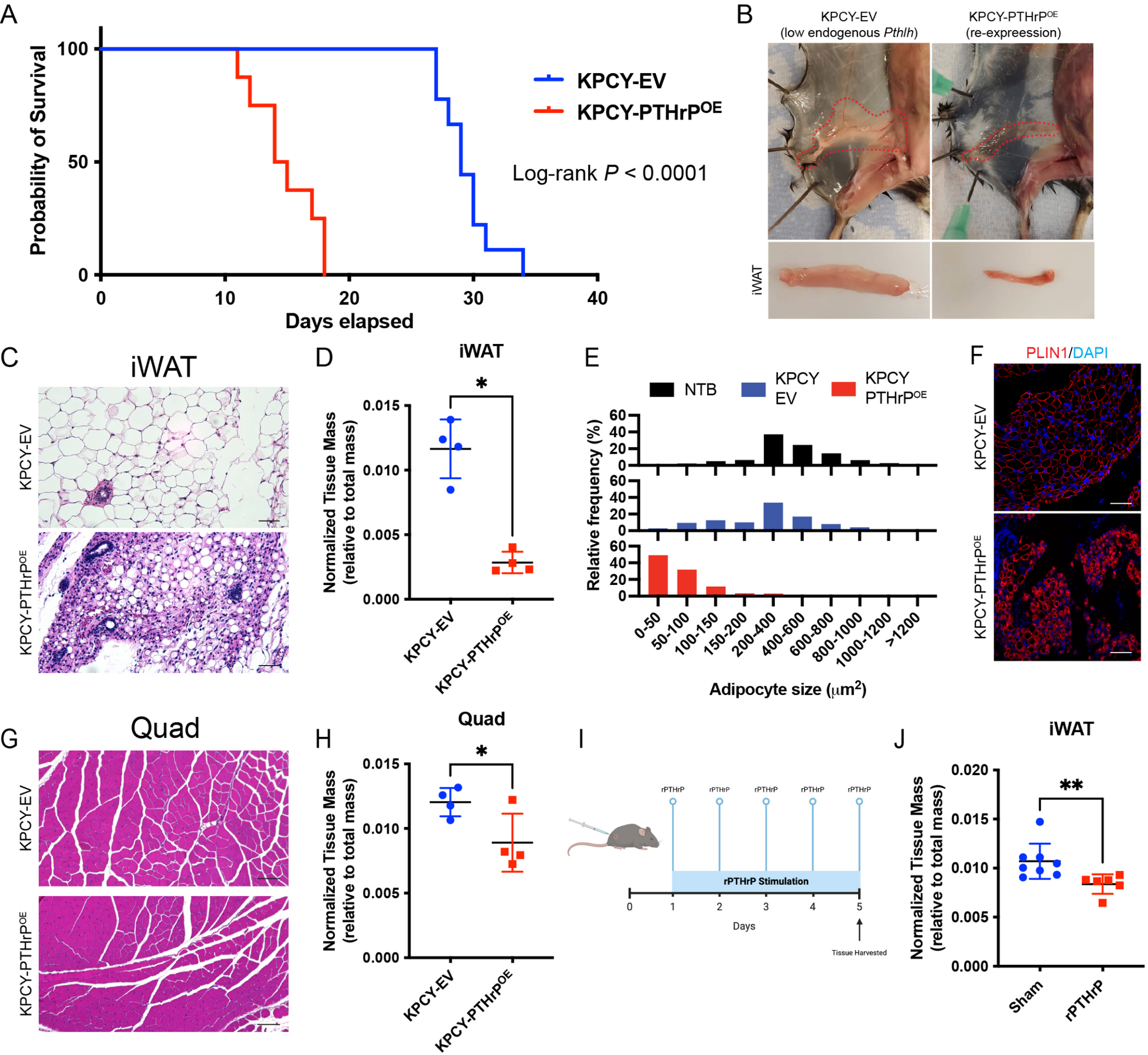
A
Probability of Survival
100
50
0
0
10
20
30
40
Days elapsed
KPCY-EV
KPCY-PTHrP^OE
Log-rank P < 0.0001
B
KPCY-EV
(low endogenous Pthlh)
KPCY-PTHrP^OE
(re-expression)
iWAT
C
iWAT
KPCY-EV
KPCY-PTHrP^OE
D
iWAT
*
Normalized Tissue Mass
(relative to total mass)
0.015
0.010
0.005
0.000
KPCY-EV
KPCY-PTHrP^OE
E
NTB
KPCY EV
KPCY PTHrP^OE
Relative frequency (%)
60
40
20
0
0-50
50-100
100-150
150-200
200-400
400-600
600-800
800-1000
1000-1200
>1200
Adipocyte size (μm²)
F
PLIN1/DAPI
KPCY-EV
KPCY-PTHrP^OE
G
Quad
KPCY-EV
KPCY-PTHrP^OE
H
Quad
*
Normalized Tissue Mass
(relative to total mass)
0.015
0.010
0.005
0.000
KPCY-EV
KPCY-PTHrP^OE
I
rPTHrP
rPTHrP
rPTHrP
rPTHrP
rPTHrP
rPTHrP Stimulation
0
1
2
3
4
5
Days
Tissue Harvested
J
iWAT
**
Normalized Tissue Mass
(relative to total mass)
0.020
0.015
0.010
0.005
0.000
Sham
rPTHrP

FIGURE 3

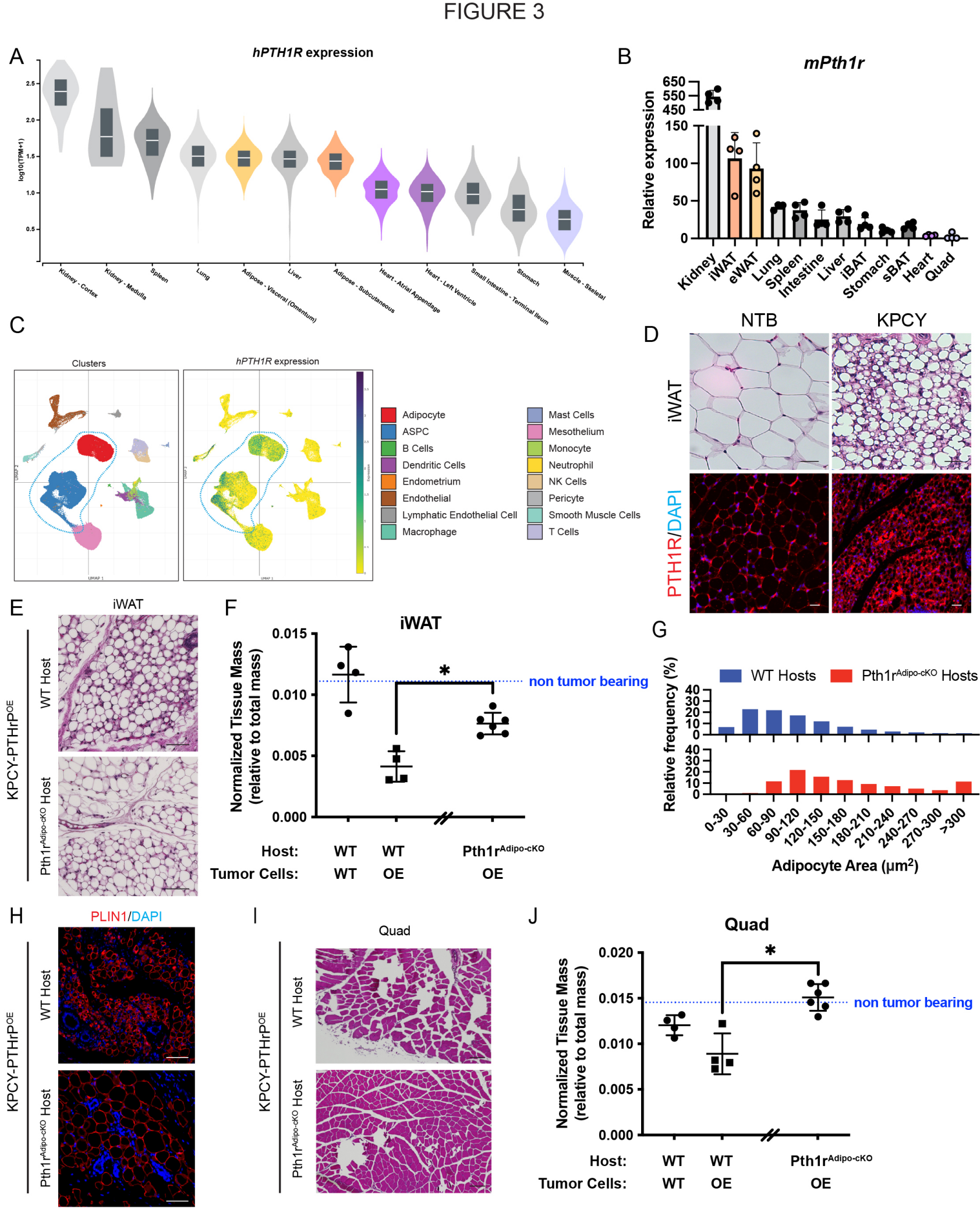
A
hPTH1R expression
log10(TPM+1)
Kidney - Cortex
Kidney - Medulla
Spleen
Lung
Adipose - Visceral (Omentum)
Liver
Adipose - Subcutaneous
Heart - Atrial Appendage
Heart - Left Ventricle
Small Intestine - Terminal Ileum
Stomach
Muscle - Skeletal
B
mPth1r
Relative expression
Kidney
iWAT
eWAT
Lung
Spleen
Intestine
Liver
iBAT
Stomach
sBAT
Heart
Quad
C
Clusters
hPTH1R expression
Adipocyte
ASPC
B Cells
Dendritic Cells
Endometrium
Endothelial
Lymphatic Endothelial Cell
Macrophage
Mast Cells
Mesothelium
Monocyte
Neutrophil
NK Cells
Pericyte
Smooth Muscle Cells
T Cells
D
NTB
KPCY
iWAT
PTH1R/DAPI
E
iWAT
KPCY-PTHrP^OE
WT Host
Pth1r^Adipo-cKO Host
F
iWAT
Normalized Tissue Mass (relative to total mass)
non tumor bearing
Host: WT WT Pth1r^Adipo-cKO
Tumor Cells: WT OE OE
G
WT Hosts
Pth1r^Adipo-cKO Hosts
Relative frequency (%)
0-30
30-60
60-90
90-120
120-150
150-180
180-210
210-240
240-270
270-300
>300
Adipocyte Area (μm²)
H
PLIN1/DAPI
KPCY-PTHrP^OE
WT Host
Pth1r^Adipo-cKO Host
I
Quad
KPCY-PTHrP^OE
WT Host
Pth1r^Adipo-cKO Host
J
Quad
Normalized Tissue Mass (relative to total mass)
non tumor bearing
Host: WT WT Pth1r^Adipo-cKO
Tumor Cells: WT OE OE

FIGURE 4

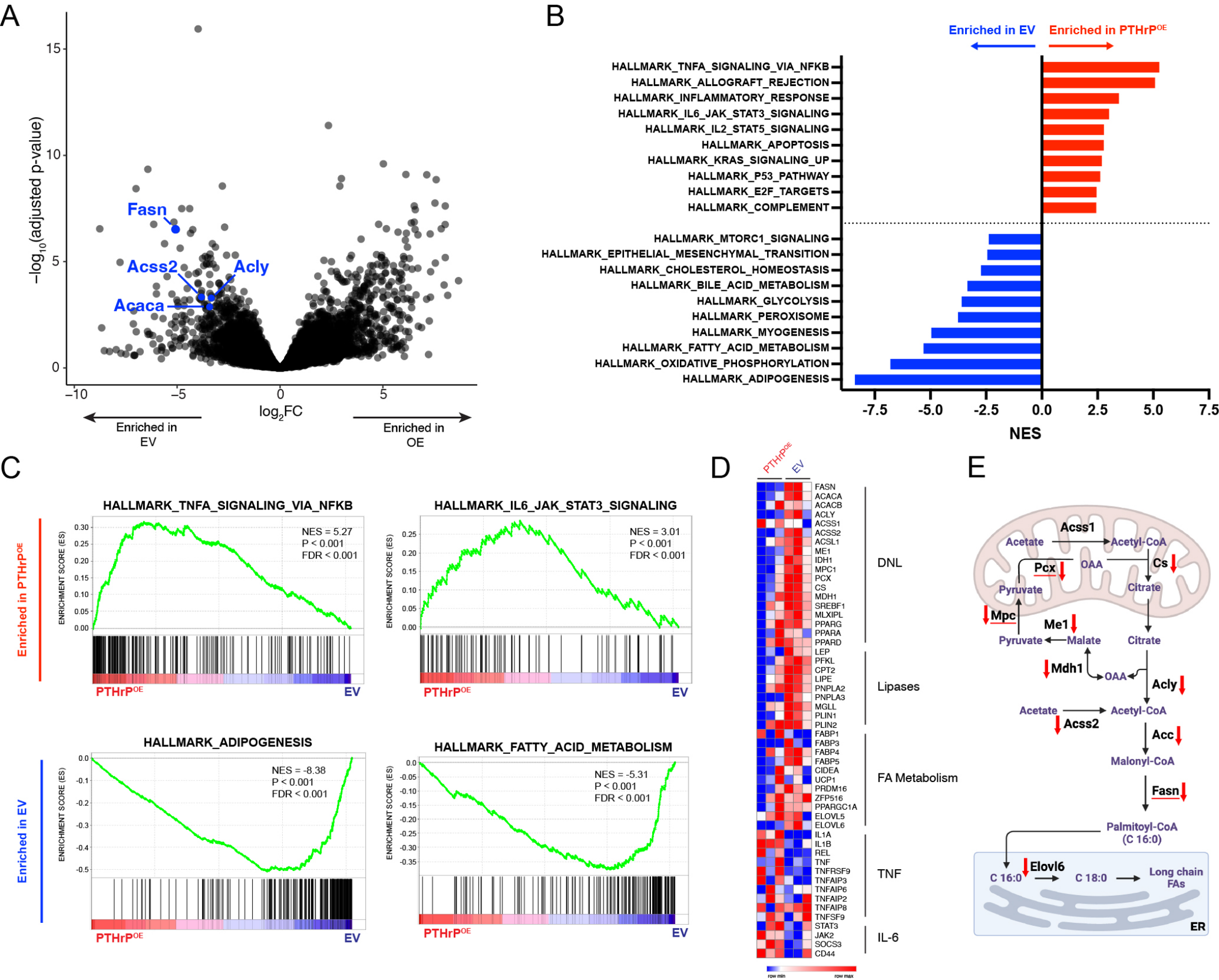
A
−log10(adjusted p-value)
log2FC
Fasn
Acss2
Acly
Acaca
Enriched in EV
Enriched in OE
B
Enriched in EV
Enriched in PTHrPOE
HALLMARK_TNFA_SIGNALING_VIA_NFKB
HALLMARK_ALLOGRAFT_REJECTION
HALLMARK_INFLAMMATORY_RESPONSE
HALLMARK_IL6_JAK_STAT3_SIGNALING
HALLMARK_IL2_STAT5_SIGNALING
HALLMARK_APOPTOSIS
HALLMARK_KRAS_SIGNALING_UP
HALLMARK_P53_PATHWAY
HALLMARK_E2F_TARGETS
HALLMARK_COMPLEMENT
HALLMARK_MTORC1_SIGNALING
HALLMARK_EPITHELIAL_MESENCHYMAL_TRANSITION
HALLMARK_CHOLESTEROL_HOMEOSTASIS
HALLMARK_BILE_ACID_METABOLISM
HALLMARK_GLYCOLYSIS
HALLMARK_PEROXISOME
HALLMARK_MYOGENESIS
HALLMARK_FATTY_ACID_METABOLISM
HALLMARK_OXIDATIVE_PHOSPHORYLATION
HALLMARK_ADIPOGENESIS
NES
C
Enriched in PTHrPOE
Enriched in EV
HALLMARK_TNFA_SIGNALING_VIA_NFKB
NES = 5.27
P < 0.001
FDR < 0.001
HALLMARK_IL6_JAK_STAT3_SIGNALING
NES = 3.01
P < 0.001
FDR < 0.001
HALLMARK_ADIPOGENESIS
NES = -8.38
P < 0.001
FDR < 0.001
HALLMARK_FATTY_ACID_METABOLISM
NES = -5.31
P < 0.001
FDR < 0.001
ENRICHMENT SCORE (ES)
PTHrPOE
EV
D
PTHrPOE
EV
FASN
ACACA
ACACB
ACLY
ACSS1
ACSS2
ACSL1
ME1
IDH1
MPC1
PCX
CS
MDH1
SREBF1
MLXIPL
PPARG
PPARA
PPARD
LEP
PFKL
CPT2
LIPE
PNPLA2
PNPLA3
MGLL
PLIN1
PLIN2
FABP1
FABP3
FABP4
FABP5
CIDEA
UCP1
PRDM16
ZFP516
PPARGC1A
ELOVL5
ELOVL6
IL1A
IL1B
REL
TNF
TNFRSF9
TNFAIP3
TNFAIP6
TNFAIP2
TNFAIP8
TNFSF9
STAT3
JAK2
SOCS3
CD44
DNL
Lipases
FA Metabolism
TNF
IL-6
E
Acetate
Acss1
Acetyl-CoA
OAA
Pcx
Cs
Pyruvate
Citrate
Mpc
Me1
Pyruvate
Malate
Citrate
Mdh1
OAA
Acly
Acetate
Acetyl-CoA
Acss2
Acc
Malonyl-CoA
Fasn
Palmitoyl-CoA
(C 16:0)
Elovl6
C 16:0
C 18:0
Long chain FAs
ER

FIGURE 5

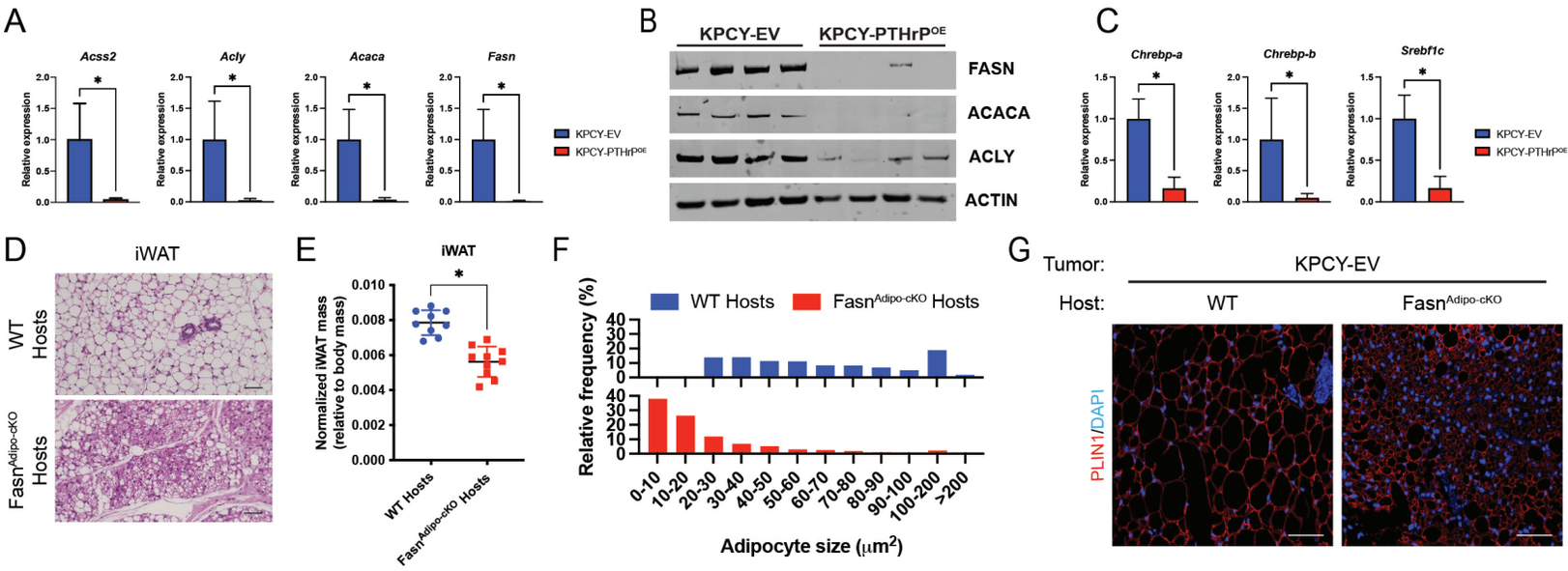
A
Acss2
Acly
Acaca
Fasn
Relative expression
KPCY-EV
KPCY-PTHrP^OE
B
KPCY-EV
KPCY-PTHrP^OE
FASN
ACACA
ACLY
ACTIN
C
Chrebp-a
Chrebp-b
Srebf1c
Relative expression
KPCY-EV
KPCY-PTHrP^OE
D
iWAT
WT Hosts
Fasn^Adipo-cKO Hosts
E
iWAT
Normalized iWAT mass (relative to body mass)
WT Hosts
Fasn^Adipo-cKO Hosts
F
WT Hosts
Fasn^Adipo-cKO Hosts
Relative frequency (%)
0-10
10-20
20-30
30-40
40-50
50-60
60-70
70-80
80-90
90-100
100-200
>200
Adipocyte size (μm²)
G
Tumor:
KPCY-EV
Host:
WT
Fasn^Adipo-cKO
PLIN1/DAPI

FIGURE 6

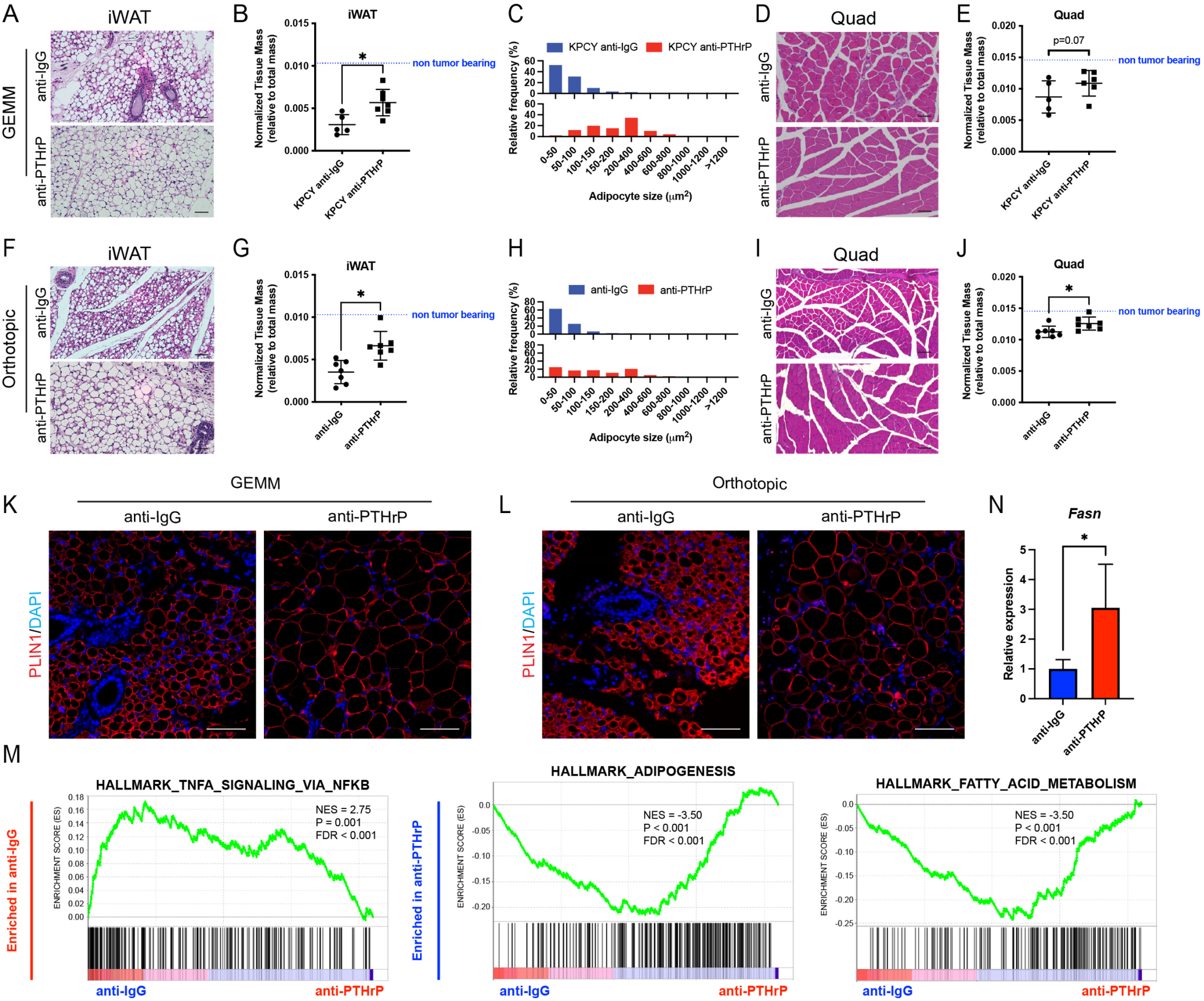
A
iWAT
GEMM
anti-IgG
anti-PTHrP
B
iWAT
Normalized Tissue Mass (relative to total mass)
non tumor bearing
KPCY anti-IgG
KPCY anti-PTHrP
C
KPCY anti-IgG
KPCY anti-PTHrP
Relative frequency (%)
Adipocyte size (μm²)
D
Quad
E
Quad
p=0.07
F
iWAT
Orthotopic
G
iWAT
H
anti-IgG
anti-PTHrP
I
Quad
J
Quad
K
GEMM
L
Orthotopic
PLIN1/DAPI
N
Fasn
Relative expression
M
HALLMARK_TNFA_SIGNALING_VIA_NFKB
NES = 2.75
P = 0.001
FDR < 0.001
Enriched in anti-IgG
HALLMARK_ADIPOGENESIS
NES = -3.50
P < 0.001
FDR < 0.001
Enriched in anti-PTHrP
HALLMARK_FATTY_ACID_METABOLISM
NES = -3.50
P < 0.001
FDR < 0.001
ENRICHMENT SCORE (ES)

FIGURE 7

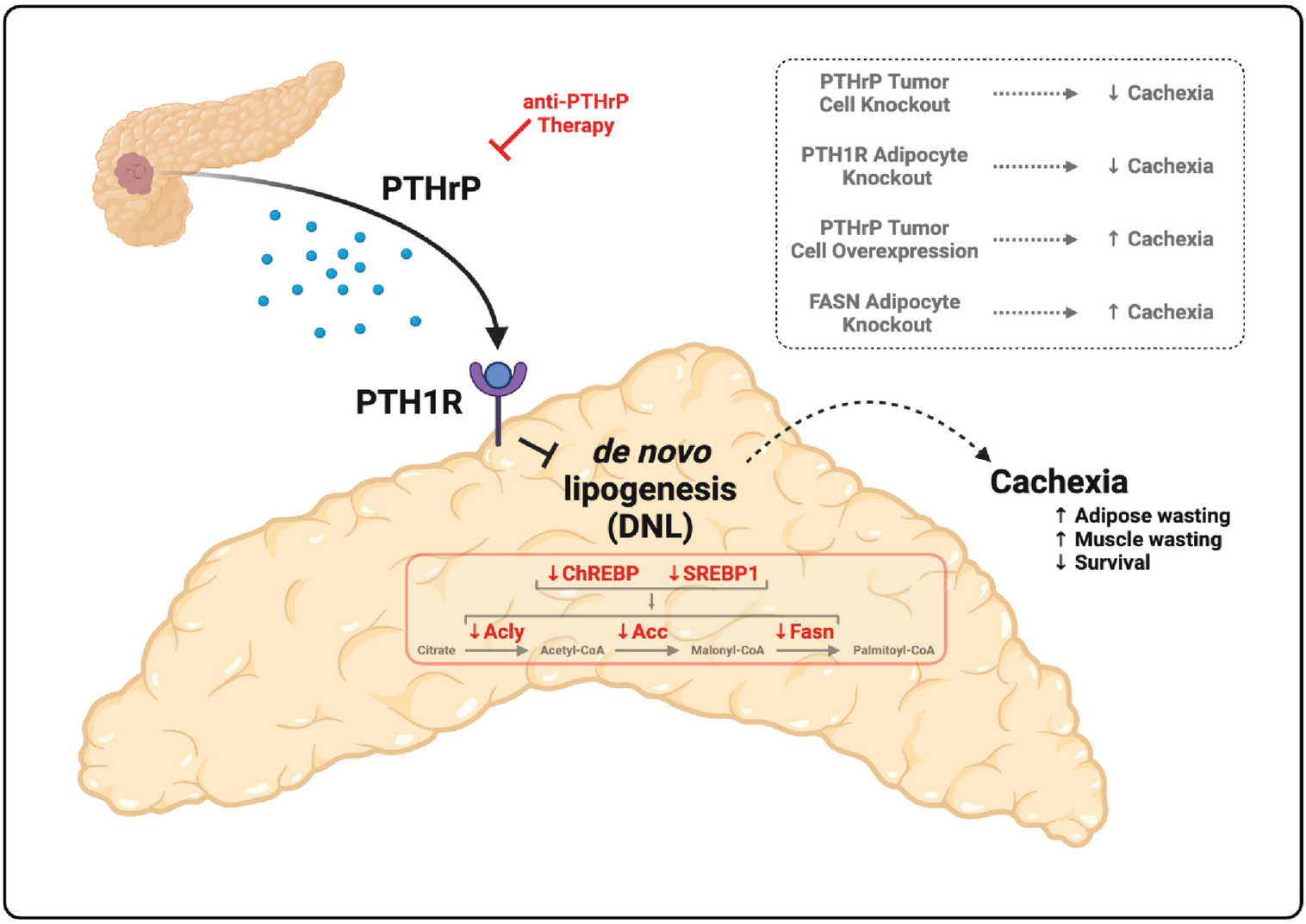
anti-PTHrP
Therapy
PTHrP
PTH1R
de novo
lipogenesis
(DNL)
↓ChREBP
↓SREBP1
↓Acly
↓Acc
↓Fasn
Citrate
Acetyl-CoA
Malonyl-CoA
Palmitoyl-CoA
PTHrP Tumor
Cell Knockout
↓ Cachexia
PTH1R Adipocyte
Knockout
↓ Cachexia
PTHrP Tumor
Cell Overexpression
↑ Cachexia
FASN Adipocyte
Knockout
↑ Cachexia
Cachexia
↑ Adipose wasting
↑ Muscle wasting
↓ Survival